ALGORITHMS FOR COLOR NORMALIZATION AND SEGMENTATION OF LIVER CANCER HISTOPATHOLOGY IMAGES

Thesis
Submitted in partial fulfillment of the requirements for the degree of

DOCTOR OF PHILOSOPHY

by

SANTANU ROY

DEPARTMENT OF ELECTRONICS & COMMUNICATION ENGINEERING

NATIONAL INSTITUTE OF TECHNOLOGY KARNATAKA
SURATHKAL, MANGALORE - 575025, INDIA

July 2020

DECLARATION

I hereby *declare* that the Research Thesis entitled **Algorithms for Color Normalization and Segmentation of Liver Cancer Histopathology Images** which is being submitted to the **National Institute of Technology Karnataka, Surathkal** in partial fulfillment of the requirements for the award of the Degree of **Doctor of Philosophy** in **Department of Electronics and Communication** is a *bona fide report of the research work carried out by me*. The material contained in this thesis has not been submitted to any University or Institution for the award of any degree.

Santanu Roy
Register No: 165089EC16F10
Department of Electronics and Communication Engineering

Place: NITK Surathkal

Date: 30-06-2021

CERTIFICATE

This is to *certify* that the Research Thesis entitled **Algorithms for Color Normalization and Segmentation of Liver Cancer Histopathology Images**, submitted by **Santanu Roy** (Register Number: 165089EC16F10) as the record of the research work carried out by him, is *accepted as a Research Thesis submission* in partial fulfillment of the requirements for the award of degree of **Doctor of Philosophy**.

Dr. Shyam Lal
Research Guide
Assistant Professor
Department Electronics and Communication Engg.
NITK Surathkal - 575025

7/07/2021
Chairman - DRPC
(Signature with Date and Seal)

This thesis is dedicated to my parents

ACKNOWLEDGEMENTS

ABSTRACT

With the advent of Computer Assisted Diagnosis (CAD), accuracy of cancer detection from histopathology images is significantly increased. However, color variation in CAD system is inevitable due to variability of stain concentration and manual tissue sectioning. Small variation in color may lead to misclassification of cancer cells. Therefore, color normalization is the first step of Computer Assisted Diagnosis (CAD), in order to reduce the inter-variability of background color among a set of source images. In this thesis, first a novel color normalization method is proposed for Hematoxylin and Eosin (H and E) stained histopathology images. Conventional Reinhard algorithm is modified in our proposed method by incorporating fuzzy logic. Moreover, mathematically it is proved that our proposed method satisfies all three hypotheses of color normalization. Furthermore, several quality metrics are estimated locally for evaluating the performance of various color normalization methods. Experimental result reveals that our proposed method has outperformed all other benchmark methods.

The second step of CAD is nuclei segmentation which is the most significant step since it enables the classification task computationally efficient and simple. However, automatic nuclei detection is fraught with problems due to highly textured nuclei boundary and various size and shapes of nuclei present in histopathology images. In this thesis, a novel edge detection technique is proposed for segmenting the nuclei regions in liver cancer Hematoxylin and Eosin (H and E) stained histopathology images, based on the notion of computing local standard deviation value. Moreover, the edge-detected image is converted into a binary image by using local Otsu thresholding and thereafter, it is refined by an adaptive morphological filter. The experimental result indicates that proposed segmentation method overcomes the limitations of existing unsupervised methods and subsequently its performance is also comparable with deep neural models. To the best of our knowledge, our proposed method is the only unsupervised method

which achieves nuclei detection accuracy closest to 1 (0.9516). Furthermore, two more quality metrics are computed in order to measure the performance of nuclei segmentation methods quantitatively. The mean value of quality metrics reveals that our proposed segmentation method outperforms other existing methods both qualitatively and quantitatively.

TABLE OF CONTENTS

LIST OF FIGURES

LIST OF TABLES

ABBREVIATIONS

ACC	Auto-Correlation Co-efficient
ACM	Active Contour Model
AMCE	Absolute Mean Color Error
ASM	Active Shape Modeling
CAD	Computer Assisted Diagnosis
CCN	Complete Color Normalization
CD	Contrast Difference
CNN	Convolutional Neural Network
FCN	Fully Convolutional Network
FMR	Fuzzy based Modified Reinhard
GHE	Global Histogram Equalization
gLoG	generalized Laplacian of Gaussian
H and E	Hematoxylin and Eosin
HS	Histogram Specification
ICA	Independent Component Analysis
JI	Jacard Index
LTE	Law's Texture Energy
LoG	Laplacian of Gaussian
MSC	Mean Shift Clustering
MSE	Mean Squared Error
MSSIM	Mean Structural Similarity Index Matrix
NMF	Non-Negative Matrix Factorization
OD	Optical Density
PCC	Pearson Correlation Co-efficient
PSNR	Peak Signal-to-noise ratio

RVM	Relevance Vector Machine
ROI	Region of Interest
SCD	Stain Color Descriptor
SEENS	Selective Edge Enhancement based Nuclei Segmentation
SNMF	Sparse Non-Negative Matrix Factorization
SPCN	Structure Preserving Color Normalization
SPV	Single path Voting
SSIM	Structural Similarity Index Matrix
SVM	Support Vector Machine
SWS	Saturated Weighted Statistics
WSI	Whole Slide Imaging

CHAPTER 1

INTRODUCTION

1.1 Introduction

Histopathology refers to the pictorial examination of tissue in order to study the cancerous disease under the microscope. In recent trends, Computer Assisted Diagnosis (CAD) has become one of the most reliable digital techniques for diagnosis and prognosis of cancer patients Gurcan et al. (2009). CAD has outperformed manual cancer detection, done by pathologists, since it is computerized and very fast and unlike manual detection, it is not dependent on human psychology. Moreover, CAD is more capable for early cancer detection than manual cancer detection, since human eye cannot extract lower order statistics. Recently in most of the hospitals (in UK and USA), CAD has been employed such that pathologists can be relieved from the huge workload and they can only focus in much difficult malignant tumour cases or in the most suspicious cases. In this research thesis, we only focus on computer assisted diagnosis of liver cancer Hematoxylin and Eosin (H and E) stained histopathology images. Hematoxylin and Eosin are the most common stains for histopathology images. Hematoxylin is mostly bound to the nuclei (bluish pink color) and Eosin is mostly bound to the cytoplasm (red pink color). There are several steps by which histopathology slides are prepared (McCann (2015), McCann et al. (2014b)) that is tissue collection, fixation, embedding, sectioning, staining and thereafter the slides are converted into digital images by Whole Slide Imaging (WSI) techniques (by Ghaznavi et al. (2013)). These digital images are called source images throughout this thesis. The preparation of histopathology slides is explained in detail in the next subsection. CAD is comprised of three steps. The first step of CAD is preprocessing (example color normalization) of histopathology images in order to reduce the inter color variation among a set of source images. Second step is to segment nuclei regions in histopathology images which is having the most

significant information of cancers, according to our pathologists' group (in Kasturba Medical College, Mangalore, MAHE). Furthermore, segmentation process enables the cancer detection task very simpler and computationally efficient. Finally, the main step of CAD is to extract features of cancer cells from segmented images and to classify whether the cell is cancerous or non-cancerous by a supervised classification technique (example Support Vector Machine, Convolutional Neural Networks). A brief description of CAD is given in section (1.3).

Generally, histopathology images are having good contrast, due to the use of advanced digital slide scanners (Olympus, Aperio, Hamamatsu etc). But those images may be faded if the tissue slides are kept for more than six months, without storing it in the computer. Thus, contrast enhancement should be done as a preprocessing step to those faded images. Color variation is another major problem of histopathology images. It may happen because of using different scanners, various staining procedures, and poor tissue sectioning (Khan et al. (2014)). Color is an important feature which is significant for cancer detection. For example, more colorful nuclei with respect to standard color may indicate the sign of malignant tumour, according to our pathologists' group (in KMC, MAHE). Thus, color normalization is very much important task prior to segmentation and classification. Small color variation might miss classify the cancer cells, which is not acceptable. The color of all the source images must be normalized to a same standard color of a reference image. This reference image must be chosen by pathologists and it is called as target image throughout this thesis. In other words, the color of this target image must be transferred to source image and after this transformation the final image will be called as processed image, throughout this thesis.

Segmentation is a very significant task before classification, since it makes the mammoth task of classification very much simple and computationally very efficient. For example, if we segment nuclei from histopathology images, then classification will be based on the features of segmented nuclei instead of features of every kind of tissues in the whole image. Thus, number of features will be significantly reduced and computational complexity of classification will be very much less, if we do segmentation prior

to classification. In this thesis, we only concentrate on segmenting nuclei regions in liver cancer H and E stained histopathology images, since most of the cancerous information contains in the nuclei region according to the pathologists (in KMC, MAHE). For example, nuclei color, variability of nuclei size and shapes, irregular boundaries all are important features of malignant tumor. However, automatic nuclei segmentation of histopathology images has been a very difficult task (Irshad et al. (2013)), for researchers because of significant size and color variation of nuclei inside one image and due to highly textured boundary present in case of higher grade cancer.

1.2 Preparing Histopathology Slides

The histopathology slides can be prepared by the following steps: 1) tissue collection, 2) fixation, 3) embedding, 4) sectioning, 5) de-paraffining, 6) staining and finally 7) digitizing the slide by Whole Slide Imaging (WSI). The schematic block diagram of histopathology slide preparation is shown in Figure 1.1.
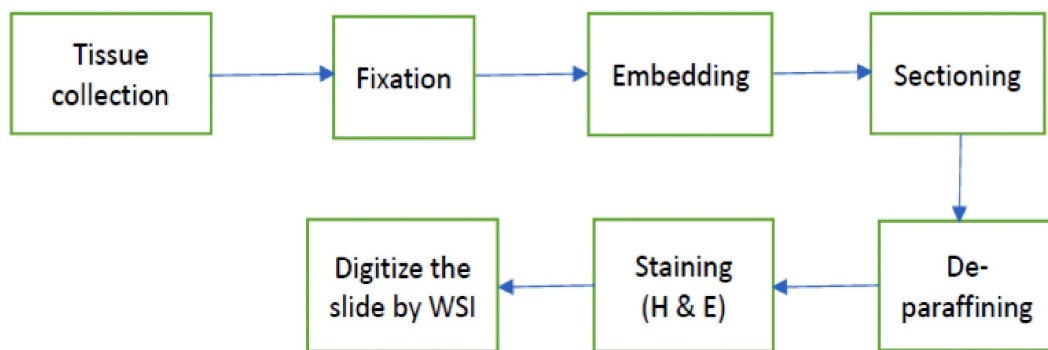
Figure 1.1: Block diagram of preparation of histopathology slides

1. Tissue Collection: There are several tissue collection methods which are fine needle aspiration, biopsy needle, excisional biopsy etc. Larger biopsy has more information than small needle biopsy because it preserves large cellular context of histopathology slides.

3

2. Fixation: Fixation of tissue is needed for chemical and physical stabilization. Mostly a combination of Alcohol and xylene are used for dry freezing (physical stability). A stabilized tissue is easier to cut by machines, thus if fixation is not done properly this may lead to poor tissue sectioning. A collection of small tissue pieces after fixation are shown in Figure 1.2a.

3. Embedding: The tissues are placed in a mold and then paraffin is poured into that mold such that those tissues will be embedded to those blocks, which are shown in Figure 1.2b. Embedding is required to give a particular shape to the tissue such that they can be easily cut by the machines.

4. Sectioning: Sectioning or cutting tissue slides into small pieces is one of the most important steps for preparing histopathology slides. Those tissues are cut by a machine or tool called microtome.Sectioning is required to get all 3-dimensional tissue information in the form of many thin slides, which is 2-dimensional information. In other words, more thinner tissue slides will provide greater information of that tissue than thick tissue slides. Although tissues are cut by machine (microtome), the orientation of the cutting is dependent on human. If the tissue slides are poorly sectioned, it may cause some information loss and color variation in histopathology slides as well as because of choosing a tilt angle it may change the orientation of the nucleus and consequently the nuclei segmentation task will be very difficult. Furthermore, if the tissue slides are cut thick, then also there will be a lots of information loss and it may generate overlapping nuclei.

5. De-paraffining: Removing paraffin from the sectioned tissue is important, without de-paraffining the tissue may look like a little bit blurry or little wet in some of the portions. To remove paraffin mostly xylene and alcohol are used.

6. Staining: Staining of the tissue slides are required because it is not visible or kind of transparent under bright field microscopy. The most widely used stains for histopathology images are Hematoxylin and Eosin. Those histopathology images are called H and E stained histopathology images. Hematoxylin stains nucleic acid and it

Figure 1.2: a.small tissue pieces after fixation, b.tissue after embedding, c.tissue section by microtome

appears as bluish pink (or blue). Mostly Hematoxylin binds to the nuclei of a cell. On the other hand, Eosin is attracted to the proteins, mostly located at the cytoplasm and appears as red/pink. Figure 1.3b shows such stained slides. The reason why Hematoxylin and Eosin are chosen is that H and E stains are attached to every cellular component of a cell which enables us to visualize the whole cellular structure of the tissue. The limitation of the H and E staining is that Hematoxylin and Eosin are mixed non-linearly in the histopathology images. That is why sometimes nuclei may look like dark purple or entirely different color (not blue), which may cause misclassification of cancer. Thus, our main challenge is to separate those two stains such that we know the color proportions of mixing at every location in the image.
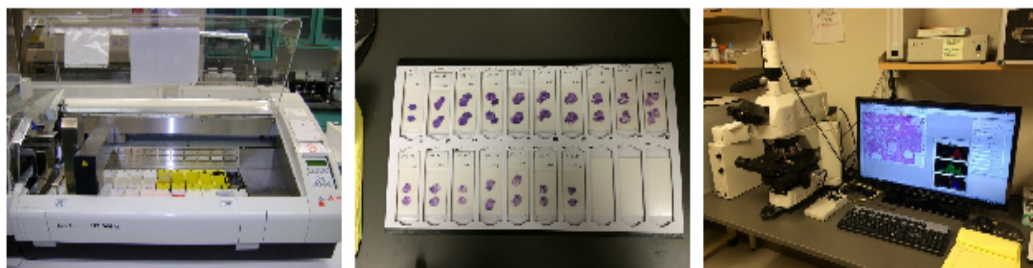
Figure 1.3: a.staining machine, b.set of slides, c.converting slides into digital slides

7. Whole Slide Imaging (WSI): Next the histopathology slides are scanned by Whole Slide Scanner and they are converted to high resolution digital images (Ghaznavi et al. (2013)), so that cancer diagnosis can be done solely by processing those digital histopathology images. Storing digital images in computer is far better option than storing histopathology slides, since glass slides can be damaged, takes more space

and can be fed over time. However, some of the pathologists still rely on analyzing the histopathology slides through microscopes because of fast focusing and virtual sense of being very much closed to the tissue. If there is any distortion in any aforementioned step, that will lead to a kind of variability (mostly in terms of color and structure) in the final digital histopathology image. In this research thesis, we mostly concern about the variability due to staining and sectioning.

1.3   Computer Assisted Diagnosis

Computer Assisted Diagnosis (CAD) is an objective or automatic pathology diagnosis which is employed in most of the hospitals in western countries. Advantage of having automatic image analysis is that it is faster than subjective pathology diagnosis and unlike subjective diagnosis it is not dependent on human psychology. Thus, for objective pathology diagnosis, the cancer detection decision does not change over the same set of histopathology images. Furthermore, the human eyes sometimes can not find the low-level textures or features for early cancer detection, which can be possible in case of Computer Assisted Diagnosis (CAD). CAD is mainly comprised of three steps, I) Pre-processing, II) segmentation, III) feature extraction and classification. The basic functional block diagram of CAD is shown in Figure 1.4.
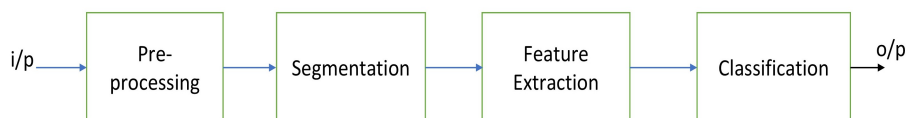
Figure 1.4: Block Diagram of CAD

1. Pre-processing: Color normalization of histopathology images is required if there is too much color variation due to different stains mix non-linearly, use of different scanners or poor tissue sectioning. Because color is an important feature of classification, little bit color variation in histopathology images may lead to misclassification (Khan et al. (2014)). Thus, color normalization is very much significant operation before segmentation and classification. The main purpose of color normalization is to transfer

6

background color from target image (standard image) to processed image, preserving all the structural information of source image.

2. Segmentation: Segmentation is nothing but partitioning the histopathology image into more meaningful regions, that is extracting the required tissue automatically (example nuclei, stroma, lymphocytes etc) which has the most significant information of cancer. Segmentation process enables the classification task simpler and it reduces its computational complexity considerably. In this thesis of liver histology, we only focused on segmenting nuclei (Yi et al. (2017), Graham et al. (2019)) since it is having the most relevant information for cancer detection. However, segmentation of nuclei in histopathology images is very challenging task, since nuclei sizes and color may vary due to stain mixing, poor tissue sectioning. Moreover, a high-grade cancer epithelial nucleus may have irregular boundary and densely cluttered. Segmenting this kind of nuclei is very difficult.

3. Feature Extraction and Classification: To classify whether the cell is cancerous or non-cancerous, first we have to extract statistical features of some tissue (Region of Interest) in the segmented H and E images. Region of Interest (ROI) can be extracted by several statistical feature extraction techniques like grey level texture feature, color based feature, Law's Texture Energy (LTE) based feature (by Kumar et al. (2015)), wavelet feature etc. Once the feature vector is created, the objects which have malignant tumour can be separated from other non-cancer objects using a linear classifier if they are linearly separable. Methods like Support vector machine (SVM) classifier (Jain et al. (2000)), Bayesian classifier (Jung et al. (2010)), KNN classifier (Jain et al. (2000)), Random Forest (Ham et al. (2005)) can be adopted to classify the cancerous cell. However, if the data are not linearly separable (or very complex to separate), Deep neural network can be employed in order to classify cancerous and non-cancerous cells. In this research, we are only focused on the first two steps of CAD, i.e. color normalization and Nuclei Segmentation.

1.4   Liver Cancer Dataset

A dataset of 75 liver cancer H and E stained histopathology images have been collected by pathologists (in KMC MAHE) for a single organ that is liver. First, histopathology slides are prepared by several steps like tissue collection, fixation, embedding, sectioning and staining. Subsequently, all the slides are visualized at same 40 x microscopic zooms, by Olympus scanner and subsequently they are converted into digital images and stored in computer. Each image size is 8.31 MB and image dimension is 1920 x 1440. According to our pathologists' group, 40 x microscopic zoom is the best suitable image for cancer detection, because at 40 x zoom nuclei size and shape are very prominent. Our dataset of liver cancer H and E stained histopathology images is one of the most challenging datasets. Because, we have observed a wide variety of image statistics all over the dataset, especially, in third grade cancer images nuclei size and shape were totally different than that of other images. However, the number of such (third grade cancer) images was only 5 in the entire dataset. Furthermore, we have noticed per 10 images, statistical properties of nuclei, other tissues and their patterns are completely different than that of other images. This happened not only because of stain variability, but also due to they are not originated from a single cell. Thus, any single automatic algorithm can not work effectively all over the dataset.

First, we need to do color normalization as a pre-processing step, since we noticed that there is significant color variation among the set of source images in the liver cancer dataset. For color normalization, we do not have any ground truth of original image, thus, it makes the color normalization task unsupervised. Moreover, in the next step of nuclei segmentation, we need a set of ground truth as well, in order to evaluate the accuracy of nuclei detection. A set of ground truth of H and E stained liver cancer histopathology images were prepared manually with the help of Adobe photoshop 2019. There is no automatic software available to generate segmented image ground truth, to the best of our knowledge. However, we found an automatic selection button which is present in photoshop 2019, has enabled us to select the exact nuclei boundary automatic, although inititally we have to choose contour manually. Thus, human error by this

method of generating ground truth is very less, according to our visualization. The nuclei are recognized by the experts (or, pathologists). In most of the cases, the nuclei appeared as blue color in H and E stained liver cancer histopathology images, since Hematoxylin stain (blue color) is mostly attracted to the nuclei. This is to clarify that we employed those set of ground truth of segmented images, just to compare it with the processed segmented image and also to measure quality metrics for nuclei detection accuracy.

1.5 Texture Property of Liver Cancer H and E Stained Histopathology Images

Texture is inherently related to the statistical (spatial) distribution of intensity values inside a local region of an image. Texture (Haralick (1979)) can be mathematically defined as follows.

$$T = \{f(x)\}_{x \in X} \tag{1.1}$$

where $f(x)$ is a probability density function inside a local patch ($x \in X$) of an image. We have found that liver cancer H and E stained histopathology images are having some unique texture properties which are discussed below.

1. In liver cancer H and E stained histopathology images, the texture property only for one feature (intensity), is approximately repeating all over the image. This kind of texture is known as periodic texture. Mathematically, an image texture will be approximately periodic if

$$f(x_i) \approx f(x_j) \forall i \neq j \tag{1.2}$$

Equation (1.2) implies that probability density function in any two patches (i^{th} and j^{th} window)in image are approximately same in case of periodic texture. However, the aforementioned property is not true for every size of patch. This patch size for which the texture is approximately periodic, actually depends on the autocorrelation co-efficient

9

of the image pixel intensity values. If auto correlation co-efficient (Haralick (1979)) is higher, then the texture will repeat after a large patch and if the reverse is true, then texture will be periodic for a small resolution patch.

2. Empirically we have found that, for liver cancer H and E stained histopathology images mostly heterogeneous property (of intensity values) dominates over homogeneity property, if the small patch size is taken greater than equal to 17 x 17, to the best of our observations. This implies that unlike natural images, histopathology image does not have a large region where intensity variation is approximately zero (example sky, tree, land etc). Statistically, in histopathology images, auto-correlation coefficient between pixel (intensity) values is comparatively greater than that of natural images. Due to this texture property, global color normalization method or any global transformation is very much suitable for histopathology images, rather than local transformation.

In order to verify the second texture property, auto-correlation co-efficient is defined below. The mathematical formula of auto-correlation co-efficient (ρ) is given in equation (1.3), inspired by the work of Haralick (1979).

$$\rho = \frac{(\frac{1}{W_1 W_2 - 1}) \sum_{m=-(W_1/2-1)}^{W_1/2-1} \sum_{n=-(W_2/2-1)}^{W_2/2-1} I(x,y) * I(x+m, y+n)}{(I(x,y))^2} \quad (1.3)$$

where $(m, n \neq 0)$, here both m and n are assumed to be odd number, $(W_1 \times W_2)$ is window size, $I(x,y)$ is the image intensity value. For both natural images and histopathology images, 17 x 17 window size is taken in order to compute autocorrelation co-efficient. This auto-correlation co-efficient (ρ), estimated in equation (1.3), is just the measurement of self-similarity of pixels for only one single window. Final auto-correlation co-efficient of entire image can be measured by the following equation (1.4).

$$\rho_{total} = \frac{1}{W} \sum_{i=1}^{W} \rho_i \quad (1.4)$$

10

where W is the total number of windows in image, (ρ) is the auto-correlation co-efficient, estimated for i^{th} window. The autocorrelation co-efficient (ACC) of 50 natural images and 50 histopathology images are estimated and compared in table-I, in order to verify the aforementioned texture property.

Table 1.1: Mean Value of ACC

for 50 histopathology images	for 50 natural images
1.084	1.024

Table 1.1 reveals that autocorrelation co-efficient of histopathology images are greater than that of natural images. This is to clarify that ACC value of histopathology images is only 0.06 greater than that of natural images, this 6 percent deviation is significant. Because with respect to a complete homogeneous image (blank image, whose $ACC = 1$), natural images' ACC value deviation is just 0.02. Thus, relative to that deviation (of 0.02), 0.06 is significant variation for histopathology images, according to our visualization. Therefore, this has been verified that auto-correlation co-efficient of histopathology images are more deviating (6 percent extra) from the value of 1, than the natural images.

1.6 Problem Statement

Design and development of algorithms for color normalization and nuclei segmentation of liver cancer histopathology images.

1.7 Research Objectives

The objectives are formulated for detecting liver cancer cells from histopathology images which are as follows.

1. To propose novel color normalization method for histopathology images and to

evaluate their performance.

2. To propose a robust segmentation method to extract nuclei and evaluate its performance on liver cancer histopathology images.

1.8 Main Contribution of the Thesis

1. A novel color normalization method based on fuzzy logic has been proposed for liver cancer H and E stained histopathology images. Still now, most of the recent color normalization methods are employing local methods for color transformation. However, we found that H and E stained histopathology images have spacial texture property that it doesn't have large region of homogeneous region unlike natural images. Thus, global color transformation is indeed more suitable than local transformation for H and E stained histopathology images. Moreover, we introduced three hypotheses for color normalization of histopathology images and later proved that our global color transformation method actually satisfies all three hypotheses for color normalization. Furthermore, we introduced three new quality metrics based on those three hypotheses and we have got the best quality metrics compared to other benchmark methods and also computation complexity of our method is considerably lesser than existing methods since we are employing global method.

2. Stain separation is a very complex and time consuming method employed by many researchers prior to color normalization. Because color transformation in RGB space yields undesirable color mixing in images, since R,G and B are not properly uncorrelated. We have observed that employing color normalization in $l\alpha\beta$ space (which employs Principal Component Analysis) does actually work, unless there is color artifact present in H and E stained histopathology images due to variability of stain concentration. Moreover, we have observed that those color artifacts are automatically removed from the histopathology images when we take only 'r' space information of color normalized image which is the first step of edge detection. Therefore, there is no need to employ time consuming stain separation methods like Non Negative Ma-

trix Factorization (NMF) which exactly reduces all the correlation between the stains Hematoxylin and Eosin. Rather, doing color normalization in $l\alpha\beta$ space and then taking 'r' space information works well for H and E stained histopathology images and it is indeed reducing computation complexity considerably than conventional stain separation methods.

3. We have proposed a novel nuclei segmentation method based on unique edge detection technique, followed by local Otsu thresholding and an adaptive morphology filter. The edge detection technique which we are employing is novel, a multi-scale edge detection method we incorporated based on computing local standard deviation. We have found that the conventional gradient based edge detection is almost inevitable of noise. Thus, instead of computing gradients (which is first difference between two pixels), we have computed standard deviation of s x s window (for liver cancer images it is 6 x 6) around each pixel. Therefore, the performance of our edge detection method is not dependent on only two pixel intensity values. Rather, it is dependent on all s x s pixels around each pixel, thus, our proposed method is less affected by noise. Thereafter, the edge detected image is processed by Otsu thresholding in order to convert the image into a binary image. Moreover, a novel adaptive morphology filter is employed in order to refine the thresholded image, since we have observed there could be many cluttered objects present in the binary thresholded image due to noise. The combination of this three methods (i.e. edge detection, Otsu's thresholding and adative morhology) is completely unsupervised and novel. Indeed, this is the only unsupervised method which detects nuclei in H and E stained histopathology images with accuracy closest to 100 percentage (95.16 percentage), to the best of our knowledge.

1.9   Organisation of the Thesis

Chapter 1 presents the introduction of our whole project i.e. Computer Assisted Diagnosis of Liver cancer H and E stained histopathology images. Chapter2 represents the literature survey of color normalization and nuclei segmentation of H and E stained

histopathology images.

In chapter 3, a novel color normalization method is proposed for H and E stained histopathology images. Moreover, unique hypotheses of color normalization method is introduced and based on those hypotheses three new quality metrics are introduced to evaluate the performance of color normalization methods.

In chapter 4, a novel unsupervised nuclei segmentation method is proposed for liver cancer H and E stained histopathology images. First, a unique edge detection method is proposed based on computing local standard deviation, in order to find the edges of nuclei in liver cancer histopathology images. Furthermore, a novel adaptive morphology filter has also been introduced as post processing.

In chapter 5, conclusion of the thesis is stated. Moreover, future work on CAD of liver cancer histopathology images has also been mentioned.

CHAPTER 2

LITERATURE SURVEY

2.1 Literature Survey of Color Normalization

Any color normalization technique must satisfy the following three hypotheses, to the best of our knowledge.

1. Color normalization technique must preserve the structure of original image or source image. Any loss of data is not acceptable.

2. Color normalization technique must transfer the background color from target (standard) image to processed image. In other words, in color space, that is $\mu_{target} \approx \mu_{proc}$

3. Contrast of the original image must be maintained in the processed image. This implies that contrast of the processed image should be always greater than equal to contrast of the original image, that is $C_{proc} \geq C_{original}$

Those three hypotheses have been explained in depth in chapter 3.

There are three types of color normalization method. A) Global color normalization in $l\alpha\beta$ space (e.g.histogram specification Gonzalez et al. (2004), Reinhard algorithm Reinhard et al. (2001)), B) Stain separation by supervised method (e.g.color deconvolution), C) Stain separation by unsupervised method (e.g. SVD by Macenko et al. (2009), NMF by Vahadane et al. (2016), ICA by Alsubaie et al. (2017)).

This is to notify that color normalization and stain separation are completely different task. One has to employ stain separation before doing color normalization. This has been observed by Ruifrok and Johnston (Ruifrok et al. (2001)) that, absorption spectra

of multiple stains (Hematoxylin and Eosin) have overlapping regions for histopathology images. In other words, Hematoxylin and Eosin stains mix non-linearly in some of the portions of histopathology images. Therefore, it is very necessary to separate those stain channel, before applying color transformation. Transferring color in RGB space may result undesired color mixing in the processed image, since R, G and B channels are not exactly uncorrelated. Hence, before normalizing color, this is essential to transform that image into a color space such that the (stain) channels will be kind of uncorrelated or independent.

2.1.1 Global Color Normalization

In general, global color normalization is done after separating color and intensity information in $l\alpha\beta$ space (Ruderman et al. (1998)), whereas l stands for luminance intensity and $\alpha\beta$ mainly contains color intensity information. In our understanding, transforming the image into $\alpha\beta$ space, is also kind of stain channel separation. However, correlation between l, α and β is not exactly zero, but very less. Histogram specification (Gonzalez et al. (2004)) is a global color normalization method, in which source image histogram is mapped with target image histogram such that both brightness and color statistics of source image will be like target image. Histogram specification follows Global Histogram Equalization (GHE) method for contrast stretching which is a kind of non-linear process. Because it forcefully stretches the histogram of source image until it will be approximately like target image histogram and consequently it sometimes may lose significant data of original image. Khan et al. (2014) report the performance of Histogram Specification in $l\alpha\beta$ channel.

Reinhard et al. (2001) preferred another global color normalization method which transfers the background color of the target image to the source image with preserving all other intensity information. This algorithm was first employed for natural images by Reinhard et al. (2001). The main limitation of this algorithm was that the target image and source image should have exactly same kind of statistics. However, this is not the same in case of histopathology images. Because of the unique texture property

of histopathology images, mentioned in the previous chapter, Reinhard algorithm is actually suitable for color normalization of histopathology images. Reinhard algorithm was also employed in $l\alpha\beta$ channel, in order to avoid the color mixing in RGB space. Reinhard algorithm is further explained in depth in chapter 3.

2.1.2   Stain Separation by Supervised Method

Before doing color normalization one has to separate the stains which mix non-linearly all over the histopathology image. According to Lambert Beer's law (Ruifrok et al. (2001)), given in equation (2.1), stain concentrations are non-linearly dependent in RGB space. Therefore, one has to first convert the image from RGB space to Optical Density (OD) space such that multiple stains will act linearly (Ruifrok et al. (2001)).

$$I_C = I_0 \exp\left(-OD_C\right) \tag{2.1}$$

where I_C is the intensity of transmitted light through histopathology slides, I_0 is the intensity of incident light on histopathology slides, OD_C is the intensity value of the image in OD space. The purpose of any stain separation method is to factorize OD space intensity value into two orthogonal matrices (Ruifrok et al. (2001)), S and D are given in equation (2.1), such that the stain channels will be kind of independent.

$$OD_C = log(\frac{I_0}{I_C}) = SD \tag{2.2}$$

where D is the stain color appearance matrix whose rows represent color basis vectors for each stains and S is the stain depth matrix whose columns represent concentration or absorption factor of each stain. A.C. Ruifrok and D.A. Johnston (Ruifrok et al. (2001)) have proposed a novel color deconvolution method, in which stain color appearance matrix was manually estimated by measuring the relative color proportion for R, G and B channel with only single stained (Hematoxylin or Eosin only) histopathology slide. Furthermore, stain depth matrix S can be easily evaluated by taking the inverse of D and multiplied by OD space intensity values, from equation (2.1). However, this method

requires some prior information of single stain color, which is not readily available in hospitals.

Khan et al. (2014) proposed a novel color normalization method which is comprised of four separate methods. First, by employing Stain Color Descriptor (SCD) global method they found overall stain color. Second, a supervised color classification method i.e. Relevance Vector Machine (RVM) has been incorporated to identify the locations where each stain is present. Thereafter, color appearance matrix and stain depth matrix are estimated from these set of classified pixels. Furthermore, a non-linear spline-based color normalization method is employed to transfer color locally from target image to source image. We believe that the SCD estimation followed by RVM to find the color appearance matrix is reliable, since it is done by a supervised learning method where single stained histopathology slides are taken as ground truth. However, due to transferring the color by a non-linear function, this algorithm can not preserve the exact shape of the source image histogram in the processed image, causing major information loss.

2.1.3 Stain Separation by Unsupervised Method

Independent Component Analysis (ICA) by Alsubaie et al. (2017) and Non-negative Matrix Factorization (NMF) methods by Rabinovich et al. (2004), both are unsupervised stain separation methods. The main advantage of unsupervised method is that there is no requirement of labelled data or ground truth of single stained histopathology images.NMF is an optimization technique which minimizes the distance between the source image and decomposed matrices (S and D), with the constraint that all coefficient of color appearance matrix must be non-negative (i.e. $S_{i,j} \geq 0$ and $D_{i,j} \geq 0$). However, NMF method is having some problem with ambiguity and has no closed form of solution. On the other hand, ICA method assumes that each stain acts independently on histopathology slides (Rabinovich et al. (2004)), which is not always true. Therefore, these methods are not practically feasible.

Table 2.1: Review of various color normalization methods for H and E stained histopathology images

Reference	Methods	Limitations
Gonzalez et al. (2004)	Histogram Specification	GHE causes data loss
Reinhard et al. (2001)	Color transfer algorithm in $l\alpha\beta$ space	In $l\alpha\beta$ space stains are not exactly separated.
Ruifrok et al. (2001)	Color Deconvolution method in OD space	To estimate color appearance matrix some prior information like single stained slide is needed which is not available.
Rabinovich et al. (2004)	Spectral decomposition by NMF, ICA	Solution of NMF are not closed, ICA assumes that each stain act separately which is not true.
Macenko et al. (2009)	In OD space find SVD and project data onto plane corresponding to its two largest singular values.	Most of the time it transfers wrong color, since it computed extreme angles empirically.
Khan et al. (2014)	specific color descriptor, RVM classification to find color of each stain, a non-linear spline function employed to transfer color	The structure of source image is ruined due to using non-linear spline function for color transfer
Li and Plataniotis (2015)	Illuminance matching method, Spectral normalization method by employing SW statistics prior to NMF	SW statistics is not a natural process, causing some color artifacts in the image
Vahadane et al. (2016)	Sparse Stain Separation of NMF, Structure preserving color normalization	computation complexity of SNMF is higher, solution of NMF may reach to local minima
Tam et al. (2016)	Centroid alignment, CLAHE	Local histogram specification doesn't work since it depends on the spatial dependency of pixels
Alsubaie et al. (2017)	ICA, wavelet decomposition	Wavelet transform doesn't make the stains independent

Macenko et al. (2009) and McCann et al. (2014a) both of them have employed same kind of stain separation method which is based on the fact that color of each pixel in

histopathology image is nothing but a linear combination of two stain vectors. The weightage of those stain vectors must be non-negative. Thus, the weightage always lies between those two stain vectors (i.e. between only Eosin and only Hematoxylin). Both of the methods tried to find a wedge of those weightage values instead of searching peaks (McCann et al. (2014a)). However, this kind of method can't always estimate the right stain vectors if strong staining variation is present in histopathology slide, according to Bejnordi et al. (2015).

In Complete Color Normalization (CCN) method, Li and Plataniotis (2015) have employed both illuminance normalization and spectral normalization. Spectral normalization method comprises of two parts I) NMF based spectral estimation, II) Spectral matching. Before applying NMF, a novel Saturation Weighted (SW) statistics method has been employed which smooth out Hue histograms and converted the image to a highly saturated image. This implies that color appearance matrix is converging into a diagonal matrix. Thus, it can reduce the solution space of NMF into a unique solution. However, according to our understating this SW statistics method is not a natural method, since it forcefully converting the image into a saturated image. Thus, undesirable color artifacts may present by their method. Furthermore, a unique spectral matching method is employed such that it preserves the entire stain depth matrix. However, this method could not preserve all the color variation of source image, since the color appearance matrix is entirely changed into a diagonal matrix, according to our visualization.

Structure Preserving Color Normalization (SPCN) method is recently proposed by Vahadane et al. (2016). First sparseness has been incorporated into the optimization equation of NMF, in order to reduce its solution space. Furthermore, a joint non-convex optimization problem is solved by incorporating block co-ordinate descent algorithm which is readily available in Sparse Modelling Software (SPAMS). However, computation complexity of Sparse NMF (SNMF) has considerably increased. Moreover, a structure preserving color normalization method has been employed in order to preserve the structure of the source image. According to our visualization, this structure only as-

sociates with the luminance intensity information of histopathology images, since only stain depth matrix is preserved by this method. Thus, color information is not exactly preserved by SPCN method, similar examples are shown in chapter 3.

Janowczyk et al. (2017) proposed a novel color normalization method based on neural network. First similar types of tissues (example stromal tissue, nuclei, lympho-cytes etc) of both source image and target image are partitioned using an unsupervised deep learning method, called sparse auto-encoder. Thereafter, an iterative learning filters are produced in this method which can optimally reconstruct the original image. Furthermore, color is transferred tissue per tissue from target image to source image, by conventional HS (Histogram Specification) method. This method is more accurate than global color normalization method, since unlike global method it does not transfer the same color to all of the pixels in image. However, computation complexity of this method is significantly greater than that of any other global color normalization method. Moreover, due to employing conventional HS method (Gonzalez et al. (2004)) for every local region, this method sometimes may bring artifacts in the processed image, which is undesirable. A review of color normalization methods are presented in Table 2.1.

2.2 Literature Survey of Nuclei Segmentation of H and E stained histopathology images

The meaning of segmentation is nothing but partitioning the image into more meaning-ful regions which have similar features. Typically, the image segmentation differs in two different ways, (a) Edge based segmentation and (b) Region based segmentation. Some of the popular region-based methods are region growing (Adams and Bischof (1994)), Otsu's thresholding (Otsu (1979)), Watershed transformation ((Vincent and Soille (1991)), Graph Cut method (Shi and Malik (2000)), Active Contour model (Kass et al. (1988)) etc. Some of the popular edge-based methods which scientists explored are Sobel Operator (Gonzalez et al. (2004)), Laplacian of Gaussian (LoG) filter , Multi-scale LoG by Al-Kofahi et al. (2009), generalized LoG by Kong et al. (2013), Canny

edge detection by Canny (1986) etc. Still now region-based method outperforms the edge-based method, because any edge detection technique failed to capture boundary of only foreground information. Rather it computes all of the strong gradients which is present inside an image and consequently the segmented image is noticeably affected by noise. On the other hand, the idea behind any region-based method is to find a region, which is homogeneous with respect to some criteria or features. The features can be intensity, color, gradient, texture etc. Thus, region-based method can separate the different regions in an image more efficiently than edge-based methods. However, some of the region-based methods (e.g. Region growing, Active Contour (Kass et al. (1988))) consume high computational complexity. Automatic segmentation of nuclei in H and E stained histopathology images is one of the most studied topics in recent trends. Two types of nuclei are mostly segmented in H and E stained histopathology images. One is Lymphocyte nuclei and the other one is Epithelial nuclei (Irshad et al. (2013)). Lymphocyte nuclei have regular shape (mostly elliptical) and smaller size than epithelial nuclei. It also has darker (blue) color and smooth boundary. A higher-grade cancer epithelial nucleus will be bigger in size than lymphocyte and may have non-uniform chromatin distribution and irregular boundaries which is known as Nuclear Pleomorphism. In other words, the texture will be very much higher in the boundary of Nuclear Pleomorphism, which is very much difficult to segment. Automatic segmentation of nuclei in histopathology images have several challenges, some of them are discussed below:

1. A higher-grade cancerous (epithelial) nucleus may have highly textured boundary (Irshad et al. (2013)). Those highly textured or irregular shaped boundary of nucleus is the significant feature of malignant tumour, which is very difficult to segment.

2. A higher-grade cancerous cell may have significant variability of nuclei shapes and sizes, according to our pathologists' group (in KMC MAHE, Manipal, India). Thus, it is a difficult problem to fix the features of nuclei, since it has no particular size and shape in histopathology images. Moreover, in some of the liver cancer H and E stained histopathology images, we found various tissues (e.g. Red Blood Cell) are having similar size and shapes with the same of nuclei, which makes the nuclei detection problem

22

further challenging.

3. Furthermore, if the histopathology slides are sectioned into thick slides (McCann et al. (2014b)), instead of perfectly equal thin slides, it may result overlapping nuclei citeal2009improved, which makes the nuclei segmentation problem very much complicated.

Nuclei segmentation is very much important task prior to classification, since it makes the mammoth task of classification computationally very efficient. The intra-variability among pixels after segmentation has been reduced considerably. Thus, the hypothesis space to find the optimal decision boundary in classification task, has been substantially reduced. Most of the segmentation techniques of H and E stained histopathology images consists of two steps A) Nuclei seed detection, B) Nuclei segmentation and boundary extraction. A review of nuclei segmentation can be found in table 2.2 and 2.3. A brief explanation is given in the following sub-section.

2.2.1 Nuclei Seed Detection

Nuclei seed detection is the first step of nuclei segmentation which is very much essential step prior to final nuclei segmentation. Generally, one seed point per nuclei is to be extracted and that point must be very much closer to nucleus center. Accuracy of nuclei segmentation in H and E stained histopathology images is heavily dependent on the accuracy of nuclei seed detection. Several researchers found difficulties to extract nuclei position because of its variability of size, shape, color and irregular boundary. Parvin et al. (2007) proposed a novel iterative voting method which is suitable for detecting the center of nuclei in a cancerous cell. First, they computed weights by Gaussian Kernel for each pixel in image and update the voting direction for a pixel towards the nearest pixel, having high gradient value. After an iterative method all the pixels, getting larger votes than a threshold value is detected as nuclei seeds. However, this method is too much time-consuming. In order to reduce the computation complexity, Qi et al. (2011) has proposed a Single Path Voting (SPV) method (rather than multi-path) in order to detect the nuclei seed position. Thereafter, Mean Shift Clustering (MSC) algorithm has

23

been incorporated to reduce redundant seed detections in a single nucleus and they are merged together to a single seed. Xu et al (Xu et al. (2014)) has further improved this voting method by aggregating the voting only along the nuclei boundary, thus it further reduces the computation complexity of voting method considerably.

Al-Kofahi et al. (2009) proposed a multi-scale LoG filter for nuclei segmentation of H and E stained histopathology images, in which they first computed the responses of LoG filters at certain set of scales $[\sigma_{min}, \ldots, \sigma_{max}]$. Subsequently, they employed Euclidian distance map in order to constrain maximum scale value while computing convolution of LoG with main image. And eventually they obtain a topographical surface R (x, z) whose maxima points indicate the nuclei centroids. The computational cost of this algorithm is very much higher and its performance is too much dependent on parameters like $\sigma_{min}, \sigma_{max}$ and a resolution parameter r. Indeed, this method is not purely automatic, since we need to modify the value of those parameters for different dataset, thus, it is not suitable for automatic nuclei segmentation. Kong et al. (Kong et al. (2013)) proposed a generalized LoG (gLoG) filters which were specially designed to detect edges of different size and shape of nuclei. This algorithm generates a set of gLoG kernels, i.e. $LoG_i(x, z; \sigma)$ [where $i = 1, 2, .., n$] having various scales and directions. Subsequently, convolution between directional gLoG and image has been performed by summing up all the response map. Advantage of this method is that computation complexity of convolution operation has been considerably reduced because of associative property of kernels (Xu et al. (2016)). Recently, (Xu et al. (2016)) proposed a nuclei segmentation method which employed similar gLoG filters for edge detection of nuclei. Furthermore, they employed Otsu's thresholding (Otsu (1979)) to convert the image into binary image which is followed by watershed transform.

2.2.2 Nuclei Segmentation and boundary extraction

All of these aforementioned methods are for nuclei seed detection. However, the final segmented image can be generated by employing some kind of hole filling algorithm like watershed, active contour etc. Watershed transformation (Vincent and Soille

([1991](#))) is a region-based segmentation, which is suitable to fill a number of holes in an image. The basic idea of Watershed came from a topographical surface. Suppose we have two basins of different sizes. First, the minima points of those basins are identified, thereafter those basins are flooded until it reaches to a critical point. At that critical point, watershed or some kind of divide lines (like dam in topographical surface) must be formed in order to separate those two regions. Several researchers (Cheng et al. (2008), Jung and Kim (2010)) employed watershed transform in order to fill the holes (of nuclei) and also to separate overlapped nuclei in H and E stained histopathology images. However, watershed transformation may lead to over-segmentation, if the initial nuclei seeds are not properly detected. J. Cheng et al (Cheng et al. (2008)) employed H minima transform in order to detect minima points (marker)efficiently and further they employed a marker-based watershed transform for final segmentation. However, the value of h is not optimized in their algorithm. Therefore, C. Jung et al. (Jung and Kim (2010)) proposed another marker-based watershed algorithm in which the value of h is optimized in the H-minima transform. H. A. Phauladi et al. (Phoulady et al. (2016)) proposed a multi-thresholding segmentation technique, which is followed by a series of morphological operations to clear the unwanted tissues or noise in H and E stained histopathology images. Recently, F. Yi et al. (Yi et al. (2017)) proposed an automatic nuclei segmentation method for liver cancer histopathology images in which first they separate Hematoxylin only stain channel from Eosin by a color deconvolution method and further they incorporated a morphological operator prior to OTSU's thresholding which is followed by a distance transform to find the initial markers of a marker controlled watershed transform. A gradient-weighted distance transform is further employed in order to refine cluttered nuclei and undesired tissues from the segmented image.

Active Contour Model (ACM) (Kass et al. (1988)) is another popular region-based segmentation algorithm in which a snake type spline or active contour grows towards the object (nuclei) boundary and it minimizes the energy of active contour with the constraint that the extracted boundary of nuclei must be smooth. However, this method has the certain limitations. I) Snake can not segment multiple objects (or, nuclei) in an

image once at a time. II) Because of its complex energy function its computational cost is much higher. III) It is not exactly an automatic method, since initially we have to draw the contour manually. S. Ali and A. Madabhushi (Ali and Madabhushi (2012)) combined Active Contour with Active Shape Modelling (ASM) via level set method (Malladi et al. (1995)), in order to preserve the perfect boundaries of nuclei in H and E stained histopathology images. All of these ACM related methods have large computation complexity, since the number of nuclei per images are considerably higher in H and E stained histopathology images. P. Huang et al. (Huang and Lai (2010)) employed marker-based watershed transform in order to obtain initial contours of nuclei. Thereafter, they incorporated conventional ACM method to segment different shapes of nuclei in liver cancer histopathology images. Plissiti et al (Plissiti and Nikou (2012)) has proposed an efficient Active Shape Model (ASM) (Malladi et al. (1995)) with a physical model which is used as a training set and can extract prior information of shape and contour of nuclei. Although this algorithm has done pretty much good job to separate heavily overlapped nuclei, it is having too much computation complexity.

Recently M. Zhao et al. (Zhao et al. (2021)) employed a novel Selective Edge Enhancement based Nuclei Segmentation (SEENS) Method for nuclei segmentation of Pap Smear Images. Similar method can also be employed for nuclei segmentation of H and E stained histopathology images. First, Region of Interests (ROIs) are extracted by selective search which is followed by two screening methods based on neighbor pixels information in a graph based segmentation. These screening steps are incorporated based on single object search and in order to reduce non-nuclei regions so that they can achieve higher accuracy of nuclei detection. Thereafter, Canny edge detection (Canny (1986)) and mathematical morphology are combinedly employed in order to extract the edge information of nuclei. Finally, the extracted edge of ROIs are grouped based on contrast. Lower contrast edge groups are edge enhanced and then segmented by Chan Vese (CV) model (Getreuer (2012)), whereas the higher contrast edge groups are directly segmented by CV model. Although this method has considerably improve the accuracy of nuclei detection for Pap Smear images, the computation complexity of their method is significantly higher than any other image processing based segmentation

methods.

Automatic nuclei segmentation is very much essential task for classifying cancerous cell, since it reduces intra-variability of some features (e.g. intensity, color, texture etc.) among pixels and consequently eliminates computation complexity in classification task significantly. However, any error in this segmentation method is not acceptable since it may lead to misclassification of cancer cells. In most of the aforementioned algorithms, there is a trade-off between segmentation accuracy and computation complexity. With higher computation, extraction of high-level textural boundary can be achieved or highly overlapped nuclei can be separated. On the other hand, with less computation there will be always difficulties to segment heterogeneous chromatin distribution of nuclei and separate clustered nuclei, since in histopathology images pixel intensity variation is comparatively higher than that of natural images, mentioned in chapter 1, section 1.5.

2.2.3 Supervised Nuclei Segmentation

All aforementioned segmentation methods, mentioned in previous subsection 2.2.1 and 2.2.2, are unsupervised methods which are simple image processing techniques. This reveals that in order to perform those methods we don't require ground truth of segmented image. Recently, several researchers attempted supervised methods in order to solve nuclei segmentation problem, since still now no unsupervised method has achieved higher accuracy of nuclei detection. Neeraj Kumar et al. Kumar et al. (2017) employed Convolutional Neural Network (CNN) to extract the boundary pixels of nuclei in H and E stained histopathology images, which is followed by a region growing method in order to fill the hole inside a nucleus. M.E. Plissiti et al. Plissiti and Nikou (2012) presented a method of separating overlapped nuclei by incorporating a novel supervised learning model which extracts local features of nuclei boundary by Active Shape Modeling (ASM) Malladi et al. (1995). In other words, they combined ASM with a supervised model and in training phase they learn the parameters of the model in vibration mode, where vibration is compared with the shape of the nuclei. Y. Song et al.

Table 2.2: Review of various nuclei segmentation methods for H and E stained histopathology images

Reference	Methods	Limitations
Parvin et al. (2007)	An iterative voting method to extract the nuclei seeds, updating the voting direction for a pixel towards the nearest pixel having high gradient value.	higher computation complexity
Dalle et al. (2009)	morphology operator dilation, followed by erosion, distance transform	In distance transform, a threshold value is chosen manually, it's not a robust method.
Cheng et al. (2008)	Marker-based Watershed algorithm, markers are extracted by an adaptive H-minima transform.	This algorithm is heavily dependent on parameter h which is not optimized.
Jung and Kim (2010)	Marker based Watershed transform, modification of H transform in which h is chosen optimally.	This algorithm assumes that all nuclei shape is elliptical which is not always true, It can't separate heavily overlapped nuclei.
Al-Kofahi et al. (2009)	Graph-cut binarization, multiscale LOG filter to find the nuclei seeds, final segmentation done by graph-cut α expansion.	performance is dependent on some parameters, thus, not a robust method.
Kong et al. (2013)	A multi-scale edge detection is done by taking convolution between directional LoG kernels and image, also known as generalized LoG	this is sensitive to noise, It is heavily dependent on some parameters
Xu et al. (2016)	adaptive threshold technique, elliptical descriptor, nuclei detected by a Single Path voting algorithm, Marker based watershed transform.	sensitive to some parameters of segmentation, doesn't work well in case of high level texture of nuclei.
Song et al. (2015)	Multiscale deep learning method to find features, Super pixels are incorporated in graph partitioning method, unsupervised clustering method to separate overlapped nuclei	computation complexity is high

Table 2.3: Review of various nuclei segmentation methods for H and E stained histopathology images

Reference	Methods	Limitations
Xing and Yang (2016)	Top-bottom hat transformation, wavelet decomposition, Multi-scale region growing segmentation, adaptive morphology along with voting mechanism	Not suitable for highly textured nuclei, not suitable for highly overlapped nuclei.
Phoulady et al. (2016)	Multi-thresholding technique to segment nuclei tissues, a series of morphology operations in order to to refine the nuclei structure.	multi-thresholding technique is dependent on a thresholding parameter, morphology operation is not adaptive, thus, it can remove significant nuclei boundary information.
Xu et al. (2016)	Employed gLoG, followed by Otsu's threshold, redundant seeds are merged by Mean Shift algorithm	gLoG is highly sensitive to noise, can't preserve high level texture of nuclei.
Kumar et al. (2017)	CNN is employed to detect nuclei edges, a threshold value is set to detect nuclei seed, a region growing algorithm to fill hole inside a nucleus.	Computational complexity of method is very much higher, nuclei detection accuracy is not very closed to 1.
Yi et al. (2017)	morphological operator followed by Otsu's thresholding, a distance transform to find the markers, a marker-controlled watershed transform, finally a gradient weighted distance transform to refine the image	didn't preserve exact nuclei boundary structure, very poor Dice Similar Co-efficient.
Naylor et al. (2018)	Identify nuclei segmentation problem as a regression task of a Euclidian distance map a fully Convolutional Network is incorporated in order to separate the overlapping nuclei.	They employed ITK software to generate ground truth. However, it's not purely automatic and dependent on hu man error.
Raza et al. (2019)	incorporates additional layer in down samling path of Unet in order to make this algo robust with noise	computation comlexity is higher

Song et al. (2015) employed a multiscale deep learning method in order to extract invariant features of nuclei. Thereafter, similar pixels are clustered (K-Means) into super

pixels and those super pixels are incorporated in a graph partitioning method in order to refine the coarse segmentation. Furthermore, an unsupervised clustering method has been adopted to separate overlapping nuclei, marker of the cluster is extracted via a distance transform.

Although Convolutional Neural Network (CNN) works efficiently for images, it doesn't work for very small dataset, because there may be problem of overfitting if number of training images are very less. O. Ronneberger et al. Ronneberger et al. (2015) first time came up with a unique solution, that is, Unet CNN, in which data augmentation is done by horizontal flip, vertical flip and random rotation. Moreoevr, due to employing sliding window mechanism by local patches, more number samples are produced than total number of training images. S.A. Raza et al. Raza et al. (2019) observed that Unet can't distinguish between nuclei and other tissues, if there are little intensity difference between cytoplasm and nuclei. Thus, they come up with a unique Micronet CNN, which incorporates an additional layer in the down sampling path, in order to preserve the weak features of nuclei which may be missed during max pooling operation. This further enables the CNN model to extract nuclei features at multiple resolution and consequently, this model becomes less sensitive to noise. P. Neylor et al. Naylor et al. (2018) identified the nuclei segmentation problem as a regression task of a Euclidian distance map and they incorporated Fully Convolutional Network (FCN), (inspired from Unet Ronneberger et al. (2015)), in order to extract nuclei with higher accuracy and less computation complexity. This method is also known as DIST, which separates the overlapping nuclei efficiently. A HoverNet deep neural model is proposed by S. Graham et al. Graham et al. (2019). They incorporated the notion of prediction on horizontal and vertical distances of every nuclear pixel from their centre of mass. This novel method has enabled them to separate clustered nuclei efficiently.

CHAPTER 3

Color Normalization of H and E Stained histopathology images

3.1 Introduction

Any Color Normalization method has three purposes, to the best of our knowledge.

(I). To reduce inter-color variability among a set of input images.

(II). To improve contrast of faded histopathology images.

(III). During color normalization, no data should be lost.

A review of color normalization and stain separation has already been introduced in chapter 2. A depth explanation of hypothesis of color normalization is presented below. Any image can be decomposed by its global mean and intensity variation with respect to global mean, given in equation (3.1), where μ_g represents global mean and $I(x,y)$ indicates the intensity of a pixel at position (x,y).

$$I(x,y) = \mu_g[I(x,y)] + (I(x,y) - \mu_g(I(x,y))) \tag{3.1}$$

The first term in equation (3.1), is just a constant value which indicates the surrounding intensity of the image. This is significant to mention that intensity of image means intensity of its brightness as well as it can be its color intensity. The second term $(I - \mu_g(I))$ in equation (3.1) is very much significant as it contains all the intensity variations of the image with respect to surrounding intensity. According to our understanding, this second term contains all the significant information of an image, which must be preserved after color normalization.

3.1.1 Hypotheses of Color Normalization

Any color normalization method must satisfy the following three hypotheses. Every hypothesis is explained below with proper justification. This is the first attempt to formulate such a mathematical hypothesis in order to evaluate the performance of any color normalization method for histopathology images.

1. Color normalization method must preserve all the information of the source image, according to our pathologists' group. This information preservation can be measured by estimating correlation co-efficient between source image and processed image. The correlation co-efficient between two random variables measures the degree of their linear correlation (Wang and Bovik (2002)). Mathematically, this is the ratio of covariance between two random variables (X and Y) to the product of their individual standard deviation which is given in equation (3.2). The first hypothesis of color normalization method is given in equation (3.2).

$$\rho_{XY} = \frac{\sigma_{XY}}{\sigma_X \sigma_Y} \simeq 1 \tag{3.2}$$

If correlation coefficient between source image (X) and processed image (Y) is exactly equal to 1, this implies that X and Y are perfectly linearly correlated. That implies,

$$Y = cX \tag{3.3}$$

where c is a real constant. Then mathematically, the probability density function (pdf) $f_Y(Y)$ of the processed image Y, can be expressed in terms of pdf $f_X(X)$ of the source image X, by the statistical formula (Papoulis and Pillai (2002)), given by equation (3.4). Here X and Y are considered as random variable.

$$f_Y(Y) = \sum_{i=1}^{n} f_X(X_i) |\frac{dX_i}{dY}| \tag{3.4}$$

where n is the number of roots of equation (3.3). By applying this statistical formula (3.4), into the equation (3.3), we get the following equation (3.5).

$$f_Y(Y) = \frac{1}{c} f_X(X) \tag{3.5}$$

Equation (3.5) reveals that the shape of the normalized histogram (pdf) of source image will remain unchanged in the processed image, since only the magnitude of pdf is scaled by a real constant c. Hence, the correlation coefficient equals to 1, implies that all the intensity variation of source image is exactly preserved in the processed image, which is very much desirable for any color normalization method. Wang and Bovik (2002) described this correlation co-efficient as a measurement of structural similarity between two grey scale images. This parameter has also been preferred as Pearson Correlation Co-efficient (PCC).

However, some of the researchers had employed discrete entropy for measuring information preservation (Celik and Tjahjadi (2011)). According to our visualization, the value of discrete entropy is just a measurement of total average information in the image. It doesn't say whether that information is relevant or irrelevant. Thus, when someone want to extract additional information from the original image (e.g. satellite images), discrete entropy will be a kind of relevant measurement. However, in case of histopathology images, our goal is not to extract enough information, rather we want to preserve all the information of source images during the color normalization process. Hence, for the histopathology images, we believe that correlation coefficient is more realistic metric than discrete entropy for evaluating the preservation of source information.

2. The second hypothesis of color normalization method is that in any color normalization method, global mean color (background color) of processed image should be equal to global mean color of target image. In other words, in color space ($\alpha\beta$ space),

$$\mu_{target} \approx \mu_{proc} \tag{3.6}$$

where μ_{target} is the mean color of target image, μ_{proc} is the mean color of processed image.

There are two ways of transferring color from target image to source image. First way is to transfer the entire color, which is composed of background color and all the color variations with respect to mean color value, given in equation (3.1). If someone transfers the entire color from target image to source image, then all the color intensity variation associated with the target image will also be copied to the source image. Therefore, it will produce color artifact in the processed image shown in Figure 3.1 and all the color variation of source image will not be preserved by this method.

The second way, is to transfer only the background color from target image to source image, while all the source color variation with respect to mean, in equation (3.1), will remain same. Thus, transferring the color by this method, can actually preserve all the source color variation in the processed image and simultaneously it can reduce the inter-variability of background color among the source images. Therefore, we are considering this second way of transferring background color from target image to source image. Reinhard method and our proposed method are similar kind of color normalization method.
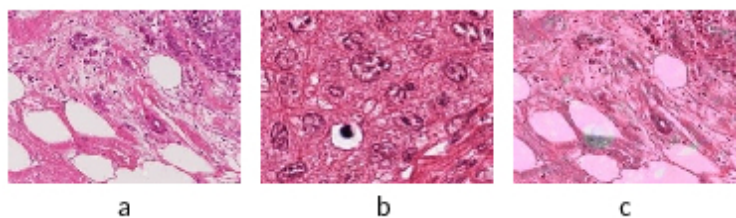
Figure 3.1: a.source image, b.target image, c.processed image

3. Contrast of the source image must be maintained in the processed image, since some of the color normalization methods may eventually reduce the contrast in the processed image [e.g. Reinhard method, SCD method]. This implies that contrast of the processed image (C_{proc}) should be always greater than the contrast of source image (C_{source}). The third hypothesis of color normalization is given by the equation (3.7).

$$C_{proc} \geq C_{Source} \qquad (3.7)$$

However, the contrast enhancement of the source image should not be unbounded.

In other words, there should not be excess or over contrast enhancement, since the histopathology images are already having good contrast, according to our observation. Moreover, due to excess contrast enhancement, nuclei color might be very much darker than the conventional nuclei color (blue) which can be interpreted as a malignant tumor, according to our pathologists' group (in KMC, Mangalore). Thus, it can misclassify the cancer cells in histopathology images. Unfortunately, we didn't find any limit or maximum contrast enhancement value theoretically. That is why, we employed a fuzzy logic technique in our proposed method, in order to control the contrast enhancement.

3.1.2 Conventional Reinhard Algorithm

In this section, we briefly introduced the pseudo code of conventional Reinhard algorithm (Reinhard et al. (2001)) which is followed by its limitations.

Pseudo Code of Reinhard Method:

Step1: Convert both of the source image X and target image Y from RGB space to $l\alpha\beta$ space (Ruderman et al. (1998)).

Step2: Do the following transformation in $l\alpha\beta$ space.

$$l_2 = \mu_g(l_1) + (l - \mu_g(l)) * (\sigma_g(l_1)/\sigma_g(l)) \tag{3.8}$$

$$a_2 = \mu_g(a_1) + (a - \mu_g(a)) * (\sigma_g(a_1)/\sigma_g(a)) \tag{3.9}$$

$$b_2 = \mu_g(b_1) + (b - \mu_g(b)) * (\sigma_g(b_1)/\sigma_g(b)) \tag{3.10}$$

Where l_2, a_2, b_2 are intensity variables of processed image in $l\alpha\beta$ space, l_1, a_1, b_1 are intensity variables of target image in $l\alpha\beta$ space and l, a, b are intensity variables of source image, μ_g indicates global mean of the image and σ_g represents global standard deviation of the image.

Step3: Convert back the processed image Z from $l\alpha\beta$ space to RGB space.

Reinhard algorithm is a global color normalization method in which all the source

intensity variation has been preserved in the processed image, since correlation co-efficient between source and processed image are found to be very much closed to 1. Moreover, the mean intensity of source image is replaced with the mean intensity of target image in all three channels, observed in equations (3.8-3.10). That is why, after this color transformation, global mean color (background color) of processed image is found to be very much closed to the same of target image. Thus, first two hypotheses of color normalization method are satisfied by Reinhard method. However, Reinhard method has certain limitations which are as follows.

1. The background luminance of source image is not preserved in the processed image, which can be observed from the equation (3.8).

2. When the source image has greater contrast than that of target image, then also it transfers the contrast statistics from target to source image, which may lead to lesser contrast of processed image than that of source image. Therefore, it doesn't satisfy the third hypothesis of color normalization.

3. Due to transferring the mean color globally from target image to source image, it transfers the same mean color to all the pixels in the image. Thus, a large homogeneous portion, associated with white luminance in the source image, can be affected by a fade color by this method. This kind of color variation is not desirable according to Khan et al. (2014) and Vahadane et al. (2016).

3.2 Proposed Color Normalization Method

In this section, Fuzzy based Modified Reinhard (FMR) method is proposed for color normalization of H and E stained histopathology images which overcome all the limitations of Reinhard method. The detailed pseudo code of FMR method is given in this section which is followed by its physical interpretation and statistical analysis.

This is important to clarify that we have employed fuzzy logic just to control the contrast enhancement in l space and to control the color co-efficients in $\alpha\beta$ space, in

order to reduce color variation. Fuzzy function is generally a mapping from a crisp set to a vague set, which makes the transformation function smoother and continuous. However, we are not interested to go back from fuzzy space to real numbers space, thus de-fuzzification is not required.

3.2.1 Fuzzy Membership Function

The fuzzy membership function which we are going to employ in our proposed method, can be generalized by one single function which is given in equation (3.11).

$$q = \varphi_1 - (\varphi_1 - \varphi_2)/(1 + exp[(p - t)/\gamma]) \qquad (3.11)$$

where q is a kind of sigmoid function whose value always lies between φ_1 and φ_2, φ_1 is the maximum value of the fuzzy function, φ_2 is the minimum value of the fuzzy function, p is a parameter defined in equation (3.12), t is the crossover point or threshold value which determines the symmetricity of the function, γ is a parameter which controls the fuzziness (smoothness) of the function. Very small value of γ means the function will become very much crispy or discrete. Greater the value of γ means the function will become smoother than the previous.
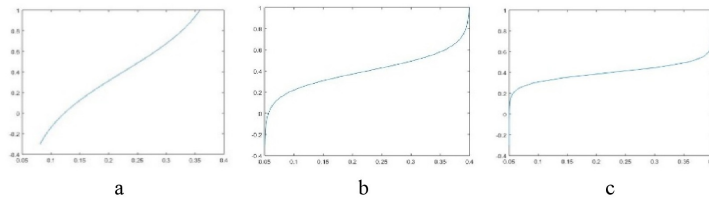
Figure 3.2: Fuzzy function q with a.$\gamma = 0.5$, b.$\gamma = 0.1$, c.$\gamma = 0.05$

The value of the parameter γ must lie between 0 to 1, When $\gamma = 1$, the fuzzy function will be tending to a straight line. In the graph in Figure 3.2, it is shown that how fuzzy function q, mentioned in equation (3.11), changes with the value of γ. Those graphs are implemented in MATLAB 2015a.

3.2.2 Estimating No of Pixels Associated with White Luminance Portion

First, the number of pixels associated with homogeneous white luminance portions are estimated locally, since the fade color effect (mentioned in the previous subsection) is directly correlated with this number of pixels. This algorithm is implemented in MATLAB 2015a, pseudo code is given in the following Algorithm 1.

Algorithm 1 Algorithm to estimate no of pixels associated with white luminance portions

---

1. h1=0
2. z=0
3. for x=0:w1:length(x)-w1
4.   x=x+1
5.   for y=0:w2:length(y)-w2
6.   y=y+1
7.   k1=0
8.   for i=0:1:(w1-1)
9.   k1=k1+1
10.   k2=0
11.   for j=0:1:(w2-1)
12.   k2=k2+1
13. $k = l(x + i, y + j)$
14.   if $(k > 0.9 * l_{max})$ and $(l_{max} >= 240)$
15.   h1=h1+1
16.   end
17.   z=z+1
18. $A(z) = l(x + i, y + j)$
19.   end
20.   end
21.   if $(std(A) > 0.5 * sqrt(mean(var(l))))$
22.   h1=h1-1
23.   end
24.   end
25. end

---

h_1 is the total number of pixels associated with homogeneous white luminance portion, the value of h_1 is normalized to h such that for any dataset, h will have same range of values (i.e. 0-100). The normalized factor of h_1 (i.e. $k_1 \times k_2$) is the window size which is same as $w_1 \times w_2$. This is important to specify that we are looking for

large (at least 35 x 39 patch) homogeneous region with only having white luminance in the source image and we have estimated the total number of pixels inside such regions. If intensity value of a single pixel in the source image is greater than $0.9 * l_{max}$ and $l_{max} > 240$ then only we increase the count of such pixels. [l_{max} is the maximum intensity in l space]. But according to our understanding, that is only the count of pixels, having luminance value closed to its maximum value. Therefore, such pixels are associated with only white luminance.

3.2.3 Proposed Fuzzy Based Modified Reinhard Method

The proposed FMR method is presented in this subsection in the form of mathematical equations. Those equations will be useful to prove hypotheses. Furthermore, a flow chart of FMR method is presented in the Figure 3.3.

Step 1: Convert both of the source image X and target image Y from RGB space to $l\alpha\beta$ space (Ruderman et al. (1998)).

Step 2: Calculate the parameter p for every source image, which is defined in equation (3.12).

$$p = \frac{\sigma_g(l_1) - \sigma_g(l)}{\sigma_g(l_1)} \tag{3.12}$$

Step 3: Define the fuzzy function s in l space: If $(p > 0)$, then execute equation (3.13), otherwise execute equation (3.14). All the parameters of fuzzy function s in equation (3.13) are chosen empirically.

$$s = 0.4 - 0.35/(1 + exp[(p - 0.4)/(0.1)]) \tag{3.13}$$

$$s = 0.05 \tag{3.14}$$

Step 4: Do the following transformation in l space. All the parameters l, l_2, μ_g were already mentioned before in previous section.

$$l_2 = \mu_g(l) + (l - \mu_g(l)) * (1 + s) \tag{3.15}$$

39

Step 5: Define the fuzzy function in color space: Store the value of h which was previously estimated in subsection 3.3.2. If $(h \geqslant 20)$, then execute equation (3.16), otherwise $q = 0$.

All the parameters of fuzzy function q in equation (3.16) are chosen empirically.

$$q = 0.3 - 0.25/(1 + exp[(h * 0.005 - 0.1)/(0.1)]) \tag{3.16}$$

Step 6: Do the following transformations in $\alpha\beta$ space: All the parameters a, a_1, a_2, b, b_1, b_2 and μ_g were already mentioned before in previous sub-section, If $(u > 0)$ and $(v > 0)$, then execute equations (3.19) and (3.20), otherwise execute equations (3.21) and (3.22) in α space and β space respectively.

$$u = \mu_g(a_1) - \mu_g(a) \tag{3.17}$$

$$v = \mu_g(b_1) - \mu_g(b) \tag{3.18}$$

$$a_2 = \mu_g(a_1) * (1 - q) + (a - \mu_g(a)) \tag{3.19}$$

$$b_2 = \mu_g(b_1) * (1 - q) + (b - \mu_g(b)) \tag{3.20}$$

$$a_2 = \mu_g(a_1) + (a - \mu_g(a)) \tag{3.21}$$

$$b_2 = \mu_g(b_1) + (b - \mu_g(b)) \tag{3.22}$$

Step 7: Convert l_2,a_2 and b_2 from $l\alpha\beta$ space (Ruderman et al. (1998)) to RGB space to get the final processed image Z.

3.2.4 Physical Interpretation of Proposed Color Normalization Method

In proposed FMR method, all the image transformations are performed in $l\alpha\beta$ space Ruderman et al. (1998), like Reinhard method (Reinhard et al. (2001)). First a parameter p is defined in equation (3.12), which is directly proportional to contrast difference between a target image and source image (Here global standard deviation of image is considered to be similar to contrast of that image according to Wang et al. (2004)). The value of p lies between $(-c)$ to 1, observed from the equation (3.12), where c is a real constant. Higher value of p indicates that the source image has very poor contrast compared to target image. Subsequently, a fuzzy function s is employed in space, which is proportional to p, given in equation (3.13). More or less the function s is equivalent to function p which is just a measurement of how much contrast should be enhanced in the processed image. This statement is further mathematically proved in the next subsection. The maximum value of fuzzy function s is chosen 0.4 empirically. For example, if p has a higher value 0.8, then also the value of s will not exceed 0.4, thus excess contrast enhancement can be controlled in the processed image by employing fuzzy function s. If p is negative (i.e. the contrast of source image is already greater than the contrast of target image), then contrast enhancement of source image is not so necessary. At that case, our proposed method enhances the contrast a very little bit (minimum value of s is 0.05 or 5 percent) which ensures that the contrast of the processed image is always greater than that of source image, because the value of s is always positive. Therefore, proposed FMR method satisfies the third hypothesis of color normalization which was not true for Reinhard method.

The other parameters of s are chosen empirically. According to our visualization, the fuzzy function s is just a mapping from a set of real numbers [-c,1] to a set of positive real numbers i.e. [0.05,0.4]. The graph of p vs s is shown in Figure 3.2, for different values of γ. According to our observation, for a particular range [0.05-0.5] of values of γ, this mapping will be non-linear. We choose the value of $\gamma = 0.1$, because we prefer non-linear mapping from p to s, since it is highly correlated with human visualization.

This is to clarify that the third hypothesis of color normalization is only dependent on single parameter s, which is fixed for all dataset and it is always positive. The other two hypotheses are not dependent on s.

One of the limitations of Reinhard method was that it does not preserve the background luminance of source images. To overcome this limitation, in proposed FMR method, the background luminance of processed image is exactly replaced by the background luminance of source image, given in equation (3.15). Therefore, background luminance of source images is exactly preserved by proposed FMR method. This is further mathematically proved in the next subsection.

Moreover, the Reinhard method has the limitation of fade color effect which was already explained in the previous subsection. This fade color effect is directly correlated with the value of h, which was estimated in the previous subsection. A fuzzy function q is employed in equation (3.16), which is proportional to the value of h. The fade color effect happens only if the global mean color differences in $\alpha\beta$ space, i.e. u and v (given in equations 3.17-3.18) both are positive and the value of q is higher, according to our observation. At that case, we are transferring less mean color [i.e. $(1-q)$ times the target mean color], given in the equations (3.19-3.20), such that fade color effect will be less. The maximum value of q is chosen 0.3 empirically given in equation (3.16), this implies that minimum 70 percent of mean color we always transfer from target image to source image. The threshold value for h is chosen 20 empirically. If $h < 20$, that means homogeneous white luminance portion is less in the image and consequently, $q = 0$. Therefore, at that case, we transfer the total mean color of the target image to the processed image, given in equations (3.21-3.22).

This is significant to clarify that this fade color effect, is depending on various parameters (like threshold values, window size) mentioned in our algorithm. However, our aim was never to remove this fade color effect completely from the processed image. White luminance homogeneous portions present in the source image, can never be perfectly preserved by proposed method, since we are globally transferring the mean color to all the pixels in the processed image. However, we just attempted to reduce

the fade color effect at a certain level, in order to increase the inter-color variability among several tissues present in histopathology images and consequently, at the next step of segmentation of those several tissues can be easily done. This is also to clarify that those white luminance homogeneous portions are mostly comprised of fat or lipid. Therefore, they have no important information regarding cancer cells and should be eliminated after segmentation. Thus, if those portions are slightly affected by a fade color in our proposed method, this won't have any consequences in the final result of cancer classification.

3.2.5 Statistical Analysis of Proposed FMR Method

A statistical analysis of proposed FMR method is presented in this subsection.

From the theory of statistics (Papoulis and Pillai (2002)), we know that

$$\sigma^2(cX + d) = c^2\sigma^2(X) \tag{3.23}$$

where X is a random variable, $\sigma^2(X)$ is the variance of X, c and d are real constants.

By taking global variance both side in equation (3.15) and by employing the statistical formula given in equation (3.23), we get

$$\sigma_g^2(l_2) = \sigma_g^2(l) * (1 + s)^2 \tag{3.24}$$

or,

$$\sigma_g(l_2) = \sigma_g(l) * (1 + s) \tag{3.25}$$

By taking the global mean both side in equation (3.15), we get

$$\mu_g(l_2) = \mu_g(\mu_g(l)) + (\mu_g(l) - \mu_g(\mu_g(l))) * (1 + s) \tag{3.26}$$

or,

$$\mu_g(l_2) = \mu_g(l) \tag{3.27}$$

From the equation (3.27), we can say that global mean intensity or background luminance of processed image is exactly same as the background luminance of source image. Thus, background luminance of source image has been exactly preserved in proposed FMR method. Therefore, first limitation of Reinhard method is resolved in the proposed FMR method.

According to the contrast definition introduced by Mukherjee and Mitra (2008), contrast of an image is given by the following equation (3.28), where σ is standard deviation of intensity values and μ is mean intensity or surrounding intensity.

$$C = \sigma/\mu \tag{3.28}$$

Similarly, global contrast of the processed image C_2 in l space can be defined by the following equation (3.29).

$$C_2 = \frac{\sigma_g(l_2)}{\mu_g(l_2)} \tag{3.29}$$

By putting the value from equation (3.25) and (3.27) into equation (3.28), we get,

$$C_2 = \frac{\sigma_g(l)}{\mu_g(l)} * (1 + s) \tag{3.30}$$

From equation (3.30), we can conclude that the contrast of the processed image is $(1+s)$ times the contrast of source image. For a particular source image, s is having only real positive value, thus equation (3.30) reveals that the contrast of processed image is always greater than that of source image. Hence, third hypothesis of color normalization has been satisfied by the proposed FMR method. Moreover, equation (3.30), reveals that s is the measure of how much contrast is enhanced in the processed image. For example, if the value of s is 0.3, equation (3.30) implies that the contrast of the processed image is enhanced by 30 percent.

Now, covariance between processed image and source image in space is given by

the equation (3.31), from covariance definition.

$$\sigma_{ll_2} = \frac{1}{MN}\sum_{i=1}^{M}\sum_{j=1}^{N}(l_{2i} - \mu_g(l_{2i})) * (l_j - \mu_g(l_j)) \tag{3.31}$$

where $M \times N$ is the image size in l space. Putting the value from equation (3.15) and (3.27), in equation (3.31) we get,

$$\sigma_{ll_2} = \frac{1}{MN}\sum_{i=1}^{M}\sum_{j=1}^{N}(l_i - \mu_g(l_i))^2 * (1 + s) \tag{3.32}$$

or,

$$\sigma_{ll_2} = \sigma_g^2(l) * (1 + s) \tag{3.33}$$

Correlation coefficient between source image and processed image in l space is given by

$$\delta = \frac{\sigma_{ll_2}}{\sigma_g(l)\sigma_g(l_2)} \tag{3.34}$$

Substituting the value from equation (3.25) and (3.33) into equation (3.34), we can get

$$\delta = 1 \tag{3.35}$$

Hence, it is proved that correlation coefficient between source image and processed image in l space is exactly equal to 1, in proposed FMR method. Moreover, it is significant to observe from equation (3.35) that, this correlation coefficient doesn't depend on any other parameter, employed in our algorithm. Thus, we can conclude that in l space, the first hypothesis is always satisfied by proposed FMR method.

Similarly, in $\alpha\beta$ space, it can be proved that proposed FMR method satisfies three of the hypotheses.

Case-I: if there is no fade color effect (if $h < 20$, $q = 0$)

By taking global variance both side in the equation (3.21) and by employing the

equation (3.23), we get

$$\sigma_g^2(a_2) = \sigma_g^2(a) \tag{3.36}$$

or,

$$\sigma_g(a_2) = \sigma_g(a) \tag{3.37}$$

similarly,

$$\sigma_g(b_2) = \sigma_g(b) \tag{3.38}$$

Taking global mean both side in equation (3.21), we get

$$\mu_g(a_2) = \mu_g(\mu_g(a_1)) + (\mu_g(a) - \mu_g(\mu_g(a))) \tag{3.39}$$

or,

$$\mu_g(a_2) = \mu_g(a_1) \tag{3.40}$$

Similarly,

$$\mu_g(b_2) = \mu_g(b_1) \tag{3.41}$$

Equations (3.40) and (3.41) reveals that the mean color of processed image is exactly equal to the mean color of target image. Hence, our proposed FMR method satisfies the second hypothesis conditionally i.e. if $h < 20$.

Now for the covariance between processed image and source image, substituting value from equations (3.21) and (3.40) in covariance equation of α space, we get

$$\sigma_{aa_2} = \frac{1}{MN} \sum_{i=1}^{M} \sum_{j=1}^{N} (a_i - \mu_g(a_i))^2 \tag{3.42}$$

or,

$$\sigma_{aa_2} = \sigma_g^2(a) \tag{3.43}$$

Similarly substituting the values from equation (3.37) and equation (3.43) into into equation (3.34), we get in α space,

$$\delta = 1 \tag{3.44}$$

Similarly, it can be proved in β space also. Thus, in $\alpha\beta$ space it is proved that correlation co-efficient between processed image and source image is exactly equal to 1, which is not dependent on any variable. Therefore, our proposed FMR method always satisfies the first hypothesis in $\alpha\beta$ space. Hence, our proposed FMR method is capable to preserve all the color variation of source image in the processed image.

Case-II: If there is fade color effect (i.e. $h \geqslant 20$, $u > 0$, $v > 0$)

By following the exactly same procedure as case-I, we can get the following equations for case-II in $\alpha\beta$ space which are given from equations (3.45-3.48).

$$\sigma_g(a_2) = \sigma_g(a) \tag{3.45}$$

$$\sigma_g(b_2) = \sigma_g(b) \tag{3.46}$$

$$\mu_g(a_2) = \mu_g(a_1) * (1 - q) \tag{3.47}$$

$$\mu_g(b_2) = \mu_g(b_1) * (1 - q) \tag{3.48}$$

Equations (3.47) and (3.48) reveals that a portion of mean color of target image is transferred to processed image and that portion is directly correlated to fuzzy function q. Thus, second hypothesis of color normalization is partially satisfied in case-II. However, maximum value of q is chosen very less (i.e. 0.3) and the number of images with $h \geqslant 20$ is also very less in both of the databases. Thus, mean color of processed image is found very much closed to mean color of target image by FMR method. For the correlation co-efficient, the proof is exactly same as the case-I.

Hence, it is proved that our proposed FMR method satisfies all three hypotheses of color normalization. Although, here we do kind of global estimation, it is quite amazing that all those results are exactly correlated with the local estimation. Local metric estimation is further discussed in the next subsection.
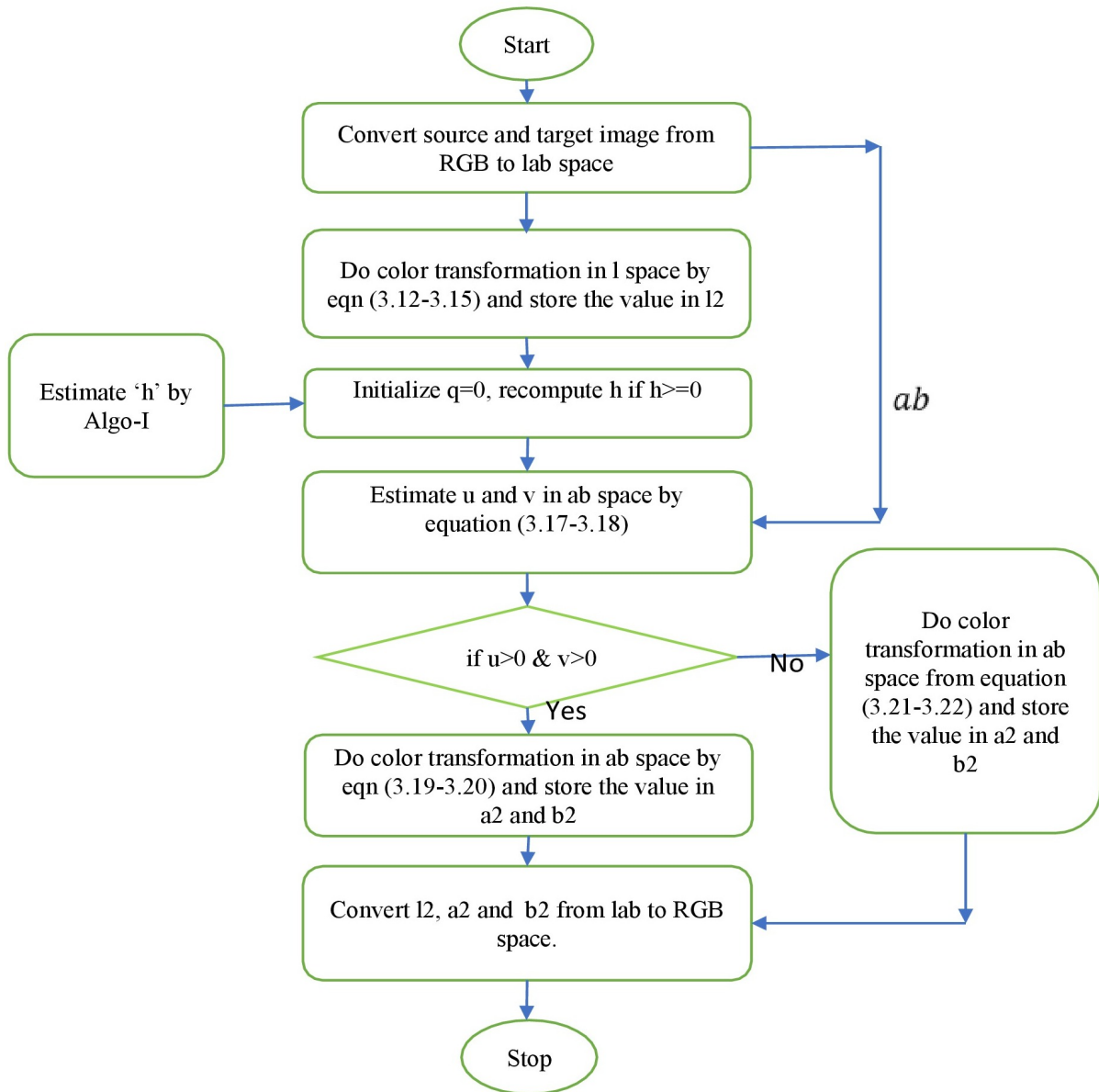
Figure 3.3: Flowchart of FMR Color Normalization Method

3.2.6 Results and Analysis

In this section, result of the proposed FMR method is compared with other existing color normalization methods such as Reinhard method (Reinhard et al. (2001)), Macenko method (Macenko et al. (2009)), SCD method (Khan et al. (2014)), CCN method (Li and Plataniotis (2015)), and SPCN method (Vahadane et al. (2016)). All the aforementioned methods were implemented and simulated with MATLAB 2015a, running on an Intel® $Core^{TM}$ i5 PC with 2.00 GHz CPU and 8 GB RAM. For experimentation,

test colon and breast cancer histopathology images are taken from publicly available databases in Khan et al. (2014) and Roux et al. (2013) respectively. And liver cancer dataset are taken from KMC, as mentioned in chapter 1. From each of the database, 80 number of images are taken for experimentation. Visual results of several color normalization algorithm are shown in Figure 3.4. Moreover, the mean values of three quality metrics for breast cancer dataset and liver dataset are resented in Table 3.1 and Table 3.2 respectively.
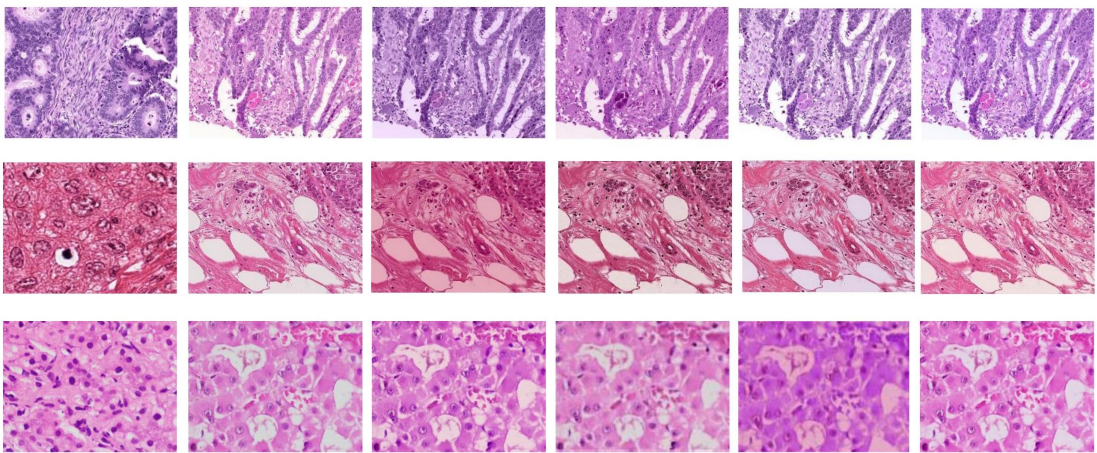
Figure 3.4: Comparison of various color normalization methods. First column represents the target images, the second column represents source images, third column represents color normalized images byReinhard et al. (2001), fourth column represents color normalized images by SCD method by Khan et al. (2014), fifth column represents color normalized images by CCN method by Li and Plataniotis (2015), sixth column represents color normalized images by SPCN method Vahadane et al. (2016), seventh column represents color normalized image by our proposed method, 1st row represents the dataset of colon cancer, 2nd row represents the dataset of breast cancer, 3rd row represents the dataset of liver cancer

A. Quality Metrics for Histopathology Images

Conventional quality metrics (e.g. Full reference metric) are not suitable for histopathology images, since the ground truth of histopathology image is not available. In fact, the ground truth is lost after the staining process, since there was color variation during staining. However, we assume that brightness intensity (gray-scale) information is entirely preserved in the source image after staining process. Thus, that grey-scale information can be extracted from the source images. The color information can be

extracted from the target image, which is preferred by pathologists. Therefore, quality of histopathology images can be evaluated by a Reduced Reference metric, where we are extracting significant information of ground truth from both source image and target image. This work is inspired from Mosquera-Lopez et al. (2015). However, we didn't choose exactly same metrics as Mosquera-Lopez et al. (2015) did. The reason behind choosing those new metrics have already been explained in section 3.1.

The following quality metrics are estimated locally. The mathematical expressions of those metrics are given below.

1. Structural similarity between source image (X) and processed image (Y) is measured by Pearson Correlation Co-efficient (PCC) and Structural Similarity Index Metric (SSIM) (Wang et al. (2004)).

$$\rho_{XY} = \frac{1}{W} \sum_{i=1}^{W} \frac{\sigma_{X_i Y_i}}{\sigma_{X_i} \sigma_{Y_i}} \tag{3.49}$$

$$SSIM(X,Y) = \frac{(2 * \mu_X \mu_X + k_1)(2 * \sigma_{XY} + k_2)}{(\mu_X^2 + \mu_Y^2 + k_1)(\sigma_X^2 + \sigma_Y^2 + k_2)} \tag{3.50}$$

$$MSSIM(X,Y) = \frac{1}{W} \sum_{i=1}^{W} SSIM(X_i, Y_i) \tag{3.51}$$

where X_i and Y_i are image contents at local i^{th} window, W is the total no. of window in image. MSSIM is the mean SSIM, σ_{XY} is the covariance between source image and processed image, σ_X is the standard deviation of X, μ_X is the mean value of X. Both of the value of k_1 and k_2 are in the order of 0.01.

2. Absolute Mean Color Error (AMCE) in both α space and β space are given in equations (3.52) and (3.53) respectively, where μ indicates local mean. α_i^{tar} is the target image content at local i^{th} window in α space and α_i^{proc} is the processed image content at local i^{th} window in α space, W is the total no of windows.

$$AMCE_\alpha = |\frac{1}{W} \sum_{i=1}^{W} \mu(\alpha_i(tar)) - \frac{1}{W} \sum_{i=1}^{W} \mu(\alpha_i(proc))| \tag{3.52}$$

$$AMCE_\beta = |\frac{1}{W}\sum_{i=1}^{W}\mu(\beta_i(tar)) - \frac{1}{W}\sum_{i=1}^{W}\mu(\beta_i(proc))| \qquad (3.53)$$

The inclusion of AMCE metric is very much significant which actually enables us to measure the background color variation in the processed image, with respect to the target image.

3. Contrast Difference (CD) between processed image and source image can be measured by the following mathematical equation (3.54), where $\sigma(Y_i)$ and $\sigma(X_i)$ are the standard deviation of processed image and source image respectively, at i^{th} window, μ is the mean value, W is the total no of windows. The definition is inspired from [29].

$$CD(Y,X) = \frac{1}{W}\sum_{i=1}^{W}\frac{\sigma(Y_i)}{\mu(Y_i)} - \frac{1}{W}\sum_{i=1}^{W}\frac{\sigma(X_i)}{\mu(X_i)} \qquad (3.54)$$

To satisfy the hypotheses of color normalization, mentioned in section 3.1, the following must be true.

- PCC or MSSIM value should be very much closed to 1.

- AMCE value both in α space and β space should be closed to zero.

- CD value should have positive sign.

The window size to compute quality metric is taken 20 x 23 and 18 x 23 for breast cancer and liver cancer datasets respectively. This window size should be dependent on the entire image size and they must be chosen optimally such that the number of zero padding will be minimum. All the hypotheses (except third) of color normalization can be verified by the Table 3.1 and Table 3.2 which are given below. However, mean values of those quality metrics don't always reflect the actual statistics. That is why, a box plot (Frigge et al. (1989)) is introduced in Figure (3.5-3.8), for only liver cancer data set (for a set of 80 images only) which shows how the data points are varying with respect to its mean value. For third hypothesis, only the sign of CD matters, its mean value is not important. Therefore, its value is not presented in Table (3.1-3.3). Rather, it can be visualized in the box plots, shown in Figure 3.8.

B. Result Evaluation and Comparisons

From Figure 3.4, it can be visualized that Reinhard method (Reinhard et al. (2001)) don't preserve the white luminance part in the processed image. However, both HS and Reinhard methods are well capable of preserving all the structural information of source image which is visualized in Figure 3.4 and also it can be observed from the Table 3.1 and Table 3.2. From Table 3.2, it is visible that Macenko method (Macenko et al. (2009)) doesn't transfer the right color from target image to processed image. In liver cancer dataset it has been found that the mean value of AMCE is 12.3 in α space and 3.5 in β space which are very much deviating from zero.

Table 3.1: Mean Values of Quality Metrics of 100 **breast** Cancer Histopathology Images for Color Normalization

Color Normalization Method	PCC	MSSIM	$AMCE_\alpha$	$AMCE_\beta$	CPU time (in sec)
HS	0.9835	0.9021	0.04	0.06	2.25
Reinhard	0.9976	0.9740	$\mathbf{3.5}e^{-14}$	e^{-14}	**2.2**
Macenko	0.9940	0.9732	1.96	2.41	5.0
SCD	0.8640	0.7963	1.17	2.32	256
CCN	0.9490	0.8910	3.26	4.27	22.5
SPCN	0.9910	0.9671	1.08	2.35	360
Proposed FMR	**0.9998**	**0.9939**	0.42	0.89	17

Table 3.2: Mean Values of Quality Metrics of 80 **Liver** Cancer Histopathology Images for Color Normalization

Color Normalization Method	PCC	MSSIM	$AMCE_\alpha$	$AMCE_\beta$	CPU time (in sec)
HS	0.9670	0.9083	0.42	0.25	2.2
Reinhard	0.9861	0.9263	$\mathbf{2.5}e^{-14}$	$\mathbf{1.1}e^{-14}$	**2**
Macenko	0.9140	0.8272	12.3	3.5	4.5
SCD	0.8861	0.8222	3.41	4.10	183
CCN	0.9579	0.9041	5.25	1.35	17.5
SPCN	0.9134	0.8591	4.56	1.05	330
Proposed FMR	**0.9970**	**0.9919**	0.42	0.23	10.0

From Figure 3.4, it can be visualized that SCD method (Khan et al. (2014)) doesn't

preserve all the source information in processed image. In fact, the loss of information in this method is greater than other benchmark methods. MSSIM by their method is found 0.79 and 0.82 for breast and liver dataset respectively, given in Table (3.1-3.2) which are very poor.

From Figure 3.4, it can be visualized that in CCN method (Li and Plataniotis (2015)), the white luminance part of source image is exactly preserved in their processed image. However, color information of source image is not exactly preserved by this algorithm which can be visualized in Figure 3.4. Thus, PCC and MSSIM are deviating from the value of 1 in case of breast cancer dataset, given in Table (3.1-3.2). Moreover, in breast cancer dataset sometimes this method brings undesired color artifacts, because Saturated Weighted Statistics (SWS) is not exactly a linear method, according to our visualization. Furthermore, in case of breast cancer dataset, mean of AMCE is very much deviating from 0. This can also be observed from Figure 3.6 and in Figure 3.7.
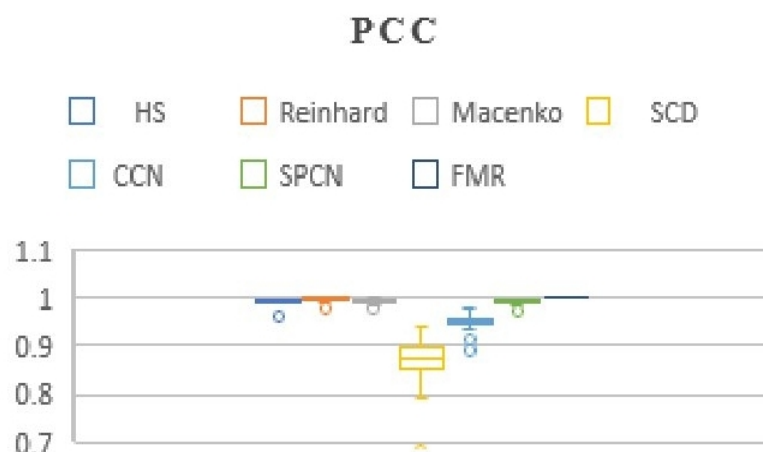
Figure 3.5: Box plot of PCC for several color normalization methods

We found only SPCN (by Vahadane et al. (2016)) method a decent existing color normalization method which has desirable quality metric values, given in Table(3.1-3.2). From Figure 3.4, it can be visualized that all the structural information of source image is preserved in the processed image, while transferring right color from target image to processed image. However, all the color variation of source image is not exactly

AMCEα
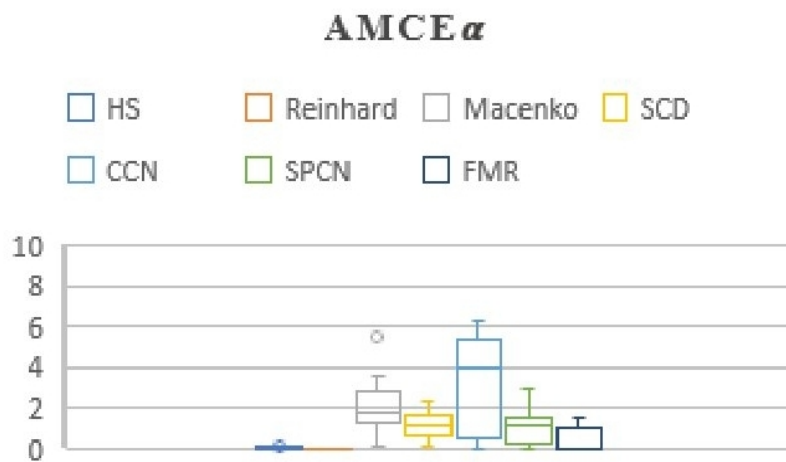
Figure 3.6: Box plot of $AMCE_\alpha$ for several color normalization methods

AMCEβ
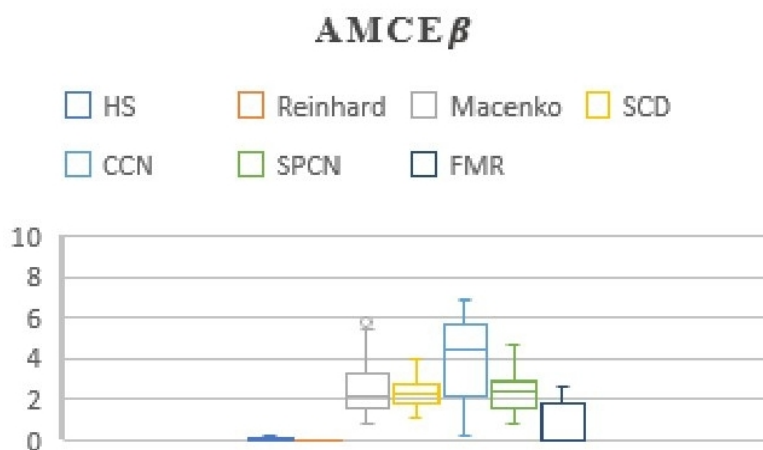
Figure 3.7: Box plot of $AMCE_\beta$ for several color normalization methods

preserved in the processed image, which can be seen in Figure 3.4. PCC and MSSIM in this method are better than CCN method, found in Table 3.1 for breast dataset. However, in liver cancer dataset it has been found that PCC and SSIM are deviating too much for SPCN method, which can be observed in Table 3.2. Therefore, there is a chance of improvement of getting better PCC or MSSIM. Another big disadvantage of this method is that it has large computation complexity, mentioned in Table (3.1-3.2). The qualitative and quantitative results reveal that our proposed FMR method outperforms all other benchmark color normalization methods.
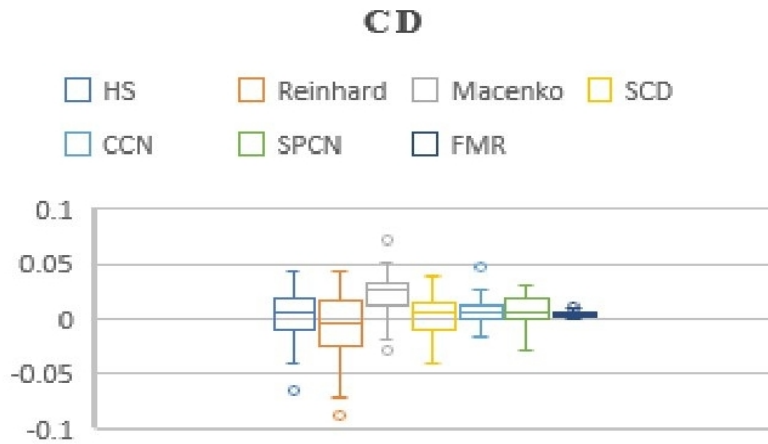
Figure 3.8: Box plot of CD for several color normalization methods

Proposed FMR method is employed to overcome all the limitations of conventional Reinhard method. In Table (3.1-3.2), it is found that FMR method has the best metric values compared to recent existing methods. It has correlation co-efficient and MSSIM value both very closed to 1, this implies that it preserves all the source information in the processed image. Subsequently, it can also be visualized from the boxplot of PCC, in Figure 3.5. Proposed FMR method has the least width in PCC boxplot, which implies that the variation of PCC value is the least in FMR method and overall PCC value is very much closed to 1. In Figure 3.4, it can be clearly observed that proposed FMR method has preserved the white luminance part of source image better than Reinhard method and HS method. However, due to the inclusion of fuzzy functions, AMCE metric values in FMR method is slightly deviating from zero, given in Table (3.1-3.2) and simultaneously it can also be observed from Figure 3.6 and Figure 3.7. But still this AMCE value for proposed FMR method is lesser than other existing algorithms except Reinhard method and HS method. Moreover, from the boxplot diagram in Figure 3.8, it is observed that CD value is always positive in proposed FMR method and it has the least width in CD boxplot which is desirable. Therefore, our proposed method satisfies the third hypothesis which was not true in Reinhard method. Furthermore, the main advantage of our proposed method is that it has very much less computation complexity compared to recent existing local methods like SCD methods and SCN methods,

which are mentioned in Table 3.1-3.2. Hence, our proposed FMR color normalization method outperformed other existing color normalization methods both qualitatively and quantitatively.

3.3 Summary

- A novel color normalization method had been proposed for liver cancer H and E stained histopathology images. Conventional Reinhard method was modified by incorporating fuzzy logic.

- Three hypotheses had been introduced for the first time, in order to evaluate color normalization of H and E stained histopathology images. Moreover, these three hyotheses were mathematically proved for our proposed color normalization method.

- Three new quality metrics were proposed for the first time in order to evaluate the performance of color normalization, based on those three hypotheses. These are reduced reference metrics, since the ground truth of original histopathology images were not readily available in nature.

CHAPTER 4

Nuclei Segmentation of Liver Cancer Histopathology Images

4.1 Introduction

In this research article, we are only focused on segmenting nuclei regions in liver cancer H and E stained histopathology images. Many researchers (Graham et al. (2019),Dalle et al. (2009) Fukuma et al. (2016)) had also focussed on only nuclei segmentation, since nuclei have the most significant information regarding cancer. However, there may be different kinds of nuclei present in the H and E stained liver cancer histopathology images, for example, some of the nuclei may belong to inflammatory cells (Cheuk et al. (2001)). Examples of inflammatory cells are endothelial cells, lymphocytes (Ishikawa et al. (2016)), neutrophils etc. Lymphocytes have comparatively darker (intensity) nuclei than epithelial nuclei, moreover, their shape is little bit circular than that of epithelial nuclei (Ishikawa et al. (2016)). This is to notify that some of the inflammatory cells (for example lymphocytes) may also carry some significant information regarding cancer (Hou et al. (2019),Galon et al. (2006)). Thus, we decided to segment all kinds of nuclei from liver cancer H and E stained histopathology images. Diffrent kinds of nuclei segmentation were already exlained in the literature survey in chapter 2, in section 2.2.2. In the following subsections, we exlained the limitations of conventional edge based segmentation methods and proposed edge detection method which is followed by post processing methods.

4.1.1 Edge-based Segmentation

Although previously we discussed that edge-based techniques have certain number of limitations over region-based methods, we have found a novel edge detection method

which overcomes the limitations of gradient based edge detection. The simplest way to find edges in an image is to take derivative with respect to space, this is also called gradient-based edge detection. Sobel operators are the first derivative of space. Whereas, Laplacian operator is the second derivative. The main limitation of 2nd derivative is that it is highly sensitive to noise. However, Laplacian operator can have more localized information of edges than 1st derivative. Therefore, Laplacian of Gaussian (LoG) filters (Gonzalez et al. (2004)) are employed by several researchers for edge detection, which is expressed in equation (4.1). Here, Gaussian filters are incorporated to reduce the noise prior to applying Laplacian operator.

$$LoG(x, z; \sigma) = \frac{\partial^2 G(x, z; \sigma)}{\partial(x)^2} \tag{4.1}$$

In equation (4.1), x, z are space co-ordinates and ∂ is the partial derivative. G is the Gaussian filter with 0 mean and σ standard deviation, represented in equation (4.2).

$$G(x, z; \sigma) = exp(-\frac{x^2 + z^2}{2\sigma^2}) \tag{4.2}$$

The main limitation of LoG filter is that it is not robust with respect to intensity variation in image. For example, some portions of an image may have higher intensity variation (means more edgy region), thus, Gaussian filter with smaller scale of σ should be chosen in order to extract fine edge details in those regions. However, noise may arise in that region if very small scale of Gaussian filter is chosen. And some portion of an image, may have small intensity variation (means homogeneous region), at that case, flatter Gaussian filter (with higher σ) should be employed in order to reduce noise. However, it may lead to large localization error of edges. Therefore, there is a trade-off between reducing noise and to keep good localization of edges (Basu (2002)). Selection of a fixed optimal scale of Gaussian filter all over the image, is a very difficult problem. Several researchers (Al-Kofahi et al. (2009), Kong et al. (2013)) have come up with the idea of multi-scale LoG filter, which were already explored in the literature survey, in Chapter-2, section 2.2.2. In both of these methods, scale of Gaussian filter is chosen manually, thus, their methods are not purely automatic and for different databases they

have to choose different parameters in their algorithm. Moreover, due to employing gradient-based method, segmented image by their method is noticeably affected by noise. We believe that in any gradient-based edge detection method, noise is inevitable. Because while taking gradient, first difference between two pixels are computed, thus, if one of the pixels is affected by noise, consequently there will be effects in their results.

Our idea was to extract edges at multi-scale automatically, but not employing any gradient-based approach. Rather we were searching for a novel concept that "the edges in the image must be proportional to some statistics of the image". Later, we observed that standard deviation is directly proportional to the edge information in image. Hence, we come up with the notion of computing local standard deviation instead of computing gradients in our novel proposed edge-detection method which is further explained in detail in the next subsection.

4.2 Proposed Nuclei Segmentation Method

Proposed nuclei segmentation method can be divided into three parts: a. Proposed Edge Detection Method, b. Otsu's Thresholding, c. Adaptive Morphology Filter.

4.2.1 Proposed Edge Detection Method

All previous edge detection methods are very much sensitive to noise and sensitive to low-level textures of image. Because, in all of the aforementioned edge detection methods gradients are computed which is finite difference between two adjacent pixels. That is why, even for small intensity variation (due to noise), those methods compute some value of gradient. Therefore, noise is inevitable, in any gradient based edge detection method. In our proposed method, edge detection is done based on computing local standard deviation in a s x s window around each pixel, mentioned in Algorithm2. Because of employing the notion of standard deviation (instead of computing gradient), our proposed method is less sensitive to noise.

Liu et al. (2000) proposed an edge detection method based on local variances. A pair of pixels whose variance is maximum in a window, only those are chosen as edges in that window. Thus, their method is neither sensitive to noise nor sensitive to lower level texture of images (Liu et al. (2000)). However, this method may lead to huge data loss in histopathology images. Because, by their method, many nuclei boundary could be open whose corresponding intensity value is not high enough, which is further shown in Figure 2. Therefore, this edge detection technique is not suitable for nuclei detection. Our work is inspired by this work, given by Liu et al. (2000). However, proposed edge detection method, is entirely different with Liu et al. (2000) and this is further explained below in depth.

Algorithm 2 Algorithm of Edge Detection in python3 opencv2

```
1. img=imread('Color Normalized Image')
2. r,g,b=cv2.spilt(img)
3. img2=nonlinearfilter(r)
4. g=20 or 40
5. def edgedetection(image):
6.    Sz=image.shape
7.    conv(img)=np.zeros(Sz)
8.    for x in range(Sz[0]-12):
9.       for z in range(Sz[1]-12):
10.          s=g*0.15
11.          sum=0
12.          st=np.std((image[x:(x+s),z:(z+s)]))
13.          for i in range(3):
14.             for j in range(3):
15.                sum=sum + (image [x+i,z+j]*(st))
16.    conv(img [x,z]) = sum
17. return conv(img)
```

Mathematical notations in Algorithm2: 'Sz' is the size of image, 'img2' is the image after non-linear filter and 'conv(img)' is the final convoluted image in the edge detection function. 'st' is the standard deviation which is chosen in 's x s' pixels around each pixels, s is correlated with g which is the magnification scale of histopathology images.

Step1: The first step of edge detection is to process only 'r' space information of color normalized image, since it mostly contains foreground information (that is nuclei),

which is observed all over the dataset.

Additionally, in 'r' space, the stains are automatically separated, which is explained later in section 4.2.2.

Step2: The 'r' space image is further processed with a non-linear filter, which is inverse logarithm ($1/log_2$) of digital Gaussian filter in 3 x 3 window. This filter reduces noise at certain level from liver cancer histopathology images.

Step3: The user has to put an input number ('g'), which is the microscopic zoom (10x, 20x or 40x) of the corresponding image. Thereafter, 'g' is multiplied by 0.15 and stored in a variable 's'. Thus, in case of 40x images, window size is 6 x 6 and in case of 20x images it is 3 x 3.

Step4: The filtered grey scale image is further convolved with a 3 x 3 mask, whose coefficients are not fixed, rather it is variable. First, we took standard deviation of sxs pixels around the first pixel in image and the same value of standard deviation is further stored in all 9 places of a 3 x 3 mask. Subsequently, corresponding pixel intensity values (in which 3 x 3 mask is being placed) is multiplied by the window coefficient and then we sum up those values in a variable 'sum' and replacing the first pixel intensity value with 'sum', as mentioned in Algorithm 1. Thereafter, this 3 x 3 window (mask) is shifted right side of the image by one step and then following the same procedure of assigning intensity values to every pixel. In this way, a convolution operation is done of entire image with that 3 x 3 mask, by employing sliding window mechanism; python code is given in Algorithm 1.

4.2.2 Physical Interpretation of Proposed Edge Detection Method

Stain separation is required before color normalization, because Ruifrok and Johnston (Ruifrok et al. (2001)) first observed that absorption spectra of multiple stains have overlapping regions (in RGB space) for histopathology images. Many researchers (Vahadane et al. (2016), Khan et al. (2014)) employed several stain separation methods which have higher computational complexity. However, we didn't employ any such
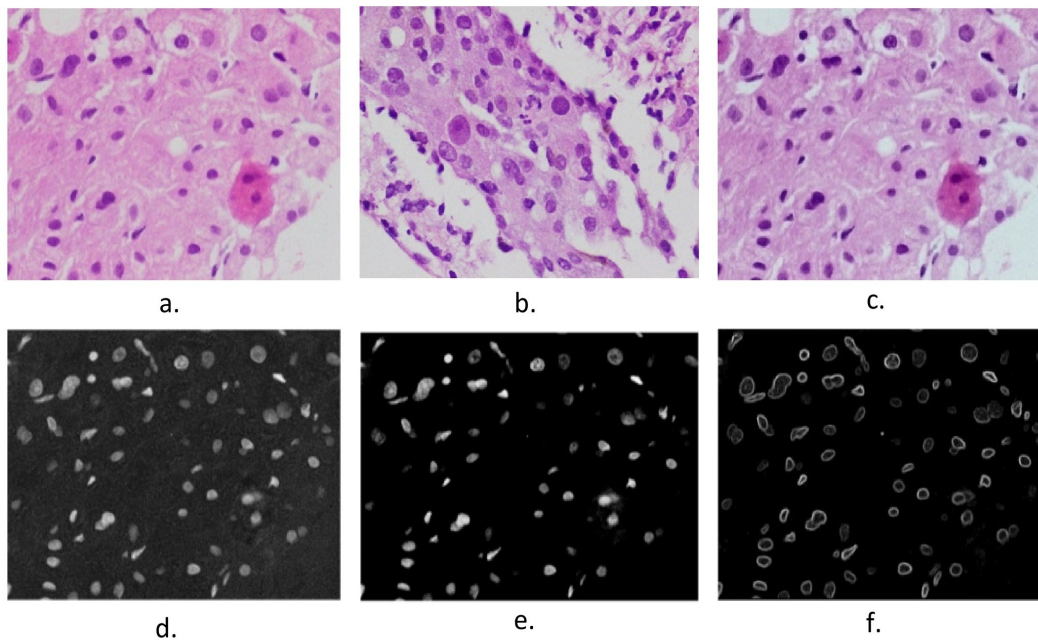
Figure 4.1: a. Source image, b. Target image, c. Color Normalized image, d.'r' space information (255-r) of color norm image, e.'r' space image after employing non-linear filter, f. Edge detected image

stain separation method in employed color normalization method. Because we observed, while converting the image from RGB to r space, in the first step of edge detection method, multiple stains are automatically separated. Figure 4.1a. is a source image, in which color artifact present due to stain variability. Subsequently, this is observed that the effect of this artifact is completely eliminated in Figure 4.1d (while taking account of only r space information) and those two nuclei are successfully recovered from that artifact. This property has been observed for all H and E stained histopathology images, which have artifacts due to stain variability. Hence, we believe that there is no need to employ stain separation method which has higher computation complexity. Rather, we just did color transformation in space, in order to avoid undesirable color mixing (in RGB space), since l, a, b channels are kind of uncorrelated (Ruderman et al. (1998))

In this reasearch, we employed a unique non-linear filter which is inverse logarithms ($1/log_2$) of 3 x 3 digital Gaussian filter. Gaussian filter has been an automatic choice for reducing noise over a decade, since this is a non-linear filter which gives more weightage to the central pixels and according to Marr and Hildreth (1980), this is the only filter which enables us to optimally localize both in space and frequency domain simul-

taneously. Moreover, due to incorporating more non-linearity (that is, taking inverse of logarithm base 2), the employed non-linear filter removes noise considerably from histopathology images which can be observed in Figure 4.1d and Figure 4.1e. The actual digital Gaussian kernel (of 3 x3 window) is given in the following equation (4.3).

$$GaussKer(3,3) = \frac{1}{16} \left\{ \begin{array}{ccc} 1 & 2 & 1 \\ 2 & 4 & 2 \\ 1 & 2 & 1 \end{array} \right\} \tag{4.3}$$

After taking $(1/log_2)$ in equation (4.3), we finally get the following kernel as employed non-linear Kernel, given in equation (4.4).

$$NonlinearKer(3,3) = 0.5 * \frac{1}{log_2} \left\{ \begin{array}{ccc} 1/16 & 1/8 & 1/16 \\ 1/8 & 1/4 & 1/8 \\ 1/16 & 1/8 & 1/16 \end{array} \right\} \tag{4.4}$$

$(1/log_2)$ of digital Gaussian filter is multiplied by a normalization factor 0.5 in equation (4.4), such that the sum of all co-efficients in $NonlinearKer$ will be less than 1. Otherwise, if the sum of all co-efficients is greater than 1, then the processed image will be a very bright image and nothing will be visible.

Since local standard deviation value is directly correlated with the edge information in image, based on our observation, the proposed edge detection method can automatically extract the edges at multi-scale. Higher the value of standard deviation indicates that the region has more edge information than the region with low value of standard deviation. Therefore, those edgy regions of image are convolved with higher standard deviation value and the less edgy regions of image are convolved with lower standard deviation value. Consequently, the edge localization has been fine and the nuclei edges are efficiently preserved in the processed image. This can be further observed in Fig.2. Moreover, this is to clarify that, images with different microscopic zoom (e.g. 20x, 40x) need different window size for calculating local standard deviation, because in 20x images nuclei are denser and smaller in size than that of 40x images. Hence, in

order to extract the edges at multiscale, window size (sxs) must be adaptive with the microscopic zoom (20x or 40x) of images. Therefore, a parameter 'g' is introduced in proposed algorithm, in order to make this algorithm automatic.
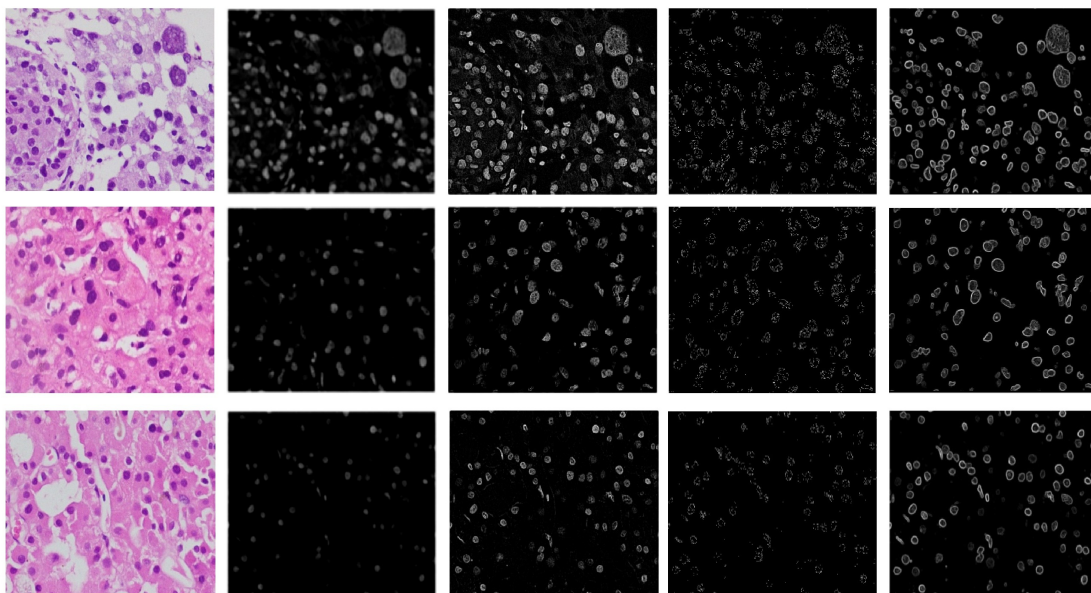
Figure 4.2: Column 1 represents source images of liver cancer histopathology images, Column 2 represents edge detected image by multi-scale LoG by Kofahi et al. Al-Kofahi et al. (2009), Column 3 represents edge detected image by gLoG Xu et al. (2016), Column 4 represents edge detected image by L. Xinchun et al. Liu et al. (2000), Column 5 represents edge detected image by proposed edge detection method

In the 'for' loop, given in python code in Algorithm 1, $Sz[0]$ and $Sz[1]$ are subtracted by 12, so that the algorithm can't count beyond 256 x 256 pixels. This is done in order to avoid zero padding (Aghdasi and Ward (1996)), this further reduces the computation complexity of the algorithm. Moreover, the performance of this edge detection method is not dependent on any parameters, mentioned in Algorithm 1, thus, this makes the algorithm purely automatic. Only input parameter 'g' we have to provide in this algorithm, 'g' should be chosen based on the nuclei size in overall image. Mostly for 20x images (multi-organ dataset), it is chosen as 20 and for 40x images (liver cancer dataset) it is chosen as 40.

Figure 4.2 reveals that proposed edge detection method extracts edges of nuclei more efficiently than other conventional edge detection methods. Moreover, this can be

further observed from Figure 4.2, that noise is very much less by proposed edge detection method, comparative to any other conventional gradient based methods. To prove that statement, a mathematical analysis is given in the following subsection. Furthermore, a quality metric Peak Signal to Noise Ratio (PSNR) between ground truth and final processed (or segmented) image, is computed in section 7, in order to support that statement experimentally.

4.2.3 Mathematical Analysis

Mathematically, our proposed edge detection operator E can be expressed by the following equation (4.5).

$$E_p = [N(x,z;\sigma_n)] * \sum_{l=1}^{W} \sum_{i=1}^{3} \sum_{j=1}^{3} I_l(x+i, z+j) * \sigma(I_l[x:x+s, z:z+s]) \qquad (4.5)$$

Here $N(x,z;\sigma_n)$ is the non-linear filter which is $(1/log_2)$ of Gaussian filter in a fixed scale σ_n, (that is 3 x 3), W is the total number of 3 x 3 windows in entire image, $I_l(x,z)$ is the value of image intensity for l^{th} window, $'*'$ is the sign of convolution, $I_l(x:x+s, z:z+s)$ is the array of image intensity values in a sxs window, standard deviation σ is computed for that sxs window around each pixel $I(x,z)$. The equation (4.5) can also be reformulated in a simple equation (4.6). Let's consider a variable $'m'$ which is nothing but sxs, that is, the total number of pixels in window. For example, 40x images 'm' is 36 and for 20x images 'm' is 9.

$$E_p = N(x,z;\sigma_n) * I(x,z) * \sigma(I_l[x:x+s, z:z+s]) \qquad (4.6)$$

Here '$*'$ is the sign of convolution in equation (4.6), $I(x,z)$ is the image intensity value. This is to clarify that, this equation (4.6) is just an approximation of our edge detection operator E, mentioned in equation (4.5), which further enables us to analyze the proposed edge detection operator prominently.

LoG operators can be expressed by the following equation (4.7), which we get from

65

equation (4.1).

$$E_{LoG} = I(x,z) * [\frac{\partial^2 G(x,z;\sigma)}{\partial^2 x} + \frac{\partial^2 G(x,z;\sigma)}{\partial^2 z}] \qquad (4.7)$$

Now, let's take a window sxs and let's consider μ is the mean intensity value of all pixels inside that window. Thus, proposed edge detector in equation (4.6), can now be expanded by the following equation (4.8).

$$E_p = N(x,z;\sigma_n) * I(x,z) * \sqrt{(\mu - I(x_1,z_1)^2 ... + (\mu - I(x_s,z_s)^2} \qquad (4.8)$$

Now, assume that inside this window, only one pixel $I(x_r, z_r)$ is affected by noise. If we further expand only the standard deviation part of equation (4.8), then there will be total (2m+1) number of terms under the root, out of which only two number of terms will be related to noise affected pixel $I(x_r, z_r)$, which are given in equation (4.9).

$$\sigma(x,z) = \sqrt{m\mu^2 - 2 * \mu[I(x_1,z_1) + ..I(x_r,z_r) + .. + I(x_s,z_s)] + ..}$$

$$\sqrt{.. + [I(x_1,z_1)^2 + .. + I(x_r,z_r)^2 + .. + I(x_s,z_s)^2} \qquad (4.9)$$

For example, in 40x images, 'm' is equal to 36, out of which only two terms will be affected by noise, thus, there will be 71 other terms (i.e. (2m-1) terms) in equation (4.9), which are independent on noise. Due to those terms, the effect of noise will be nullified in equation (4.8). Similarly, if there are two pixels affected by noise inside that window, then there will be only four terms (out of (2m+1) terms) which will be affected by noise. Thus, greater the number of terms (means larger window) in equation (4.9), causes lesser effect of noise by the proposed edge detector. However, we can't choose the window size (sxs) very large in order to avoid noise, otherwise, there will be problem of localization of edges (Canny (1986)). Because, according to Canny (1986), there is a trade-off between reducing noise and having good localization of edges, thus, an uncertainty principle lies (Basu (2002)) between these two.

On the other hand, in any gradient based edge detectors, for example in LoG, both

66

of the terms in equation (4.7) are dependent on particular intensity value of pixel (x, z). Thus, if any pixel $I(x_r, z_r)$ is affected by noise, then LoG operator or any gradient-based edge operator will be directly affected by noise. Because, any gradient-based edge operator computes gradients for all pixels individually, it doesn't employ the neighbour pixels into account. Hence, we can conclude that proposed edge detector will be less affected by noise as compared to any other gradient-based edge detector, even if we don't know what is the nature of noise, present in histopathology dataset. Hence, we can conclude that the noise energy in gradient operator (N_{grad}), is always greater than the noise energy (N_{std}) in std operator or proposed edgeoperator.

Hence,

$$N_{grad} > N_{std} \tag{4.10}$$

4.2.4 Thresholding Operation

Post processing of histopathology image is needed in order to convert the edge detected image into binary image, so that it can be compared with its ground truth image, which is also in the form of binary image.

An automatic and non-parametric thresholding technique had been proposed by Otsu (Otsu (1979)) in 1979, which can optimally choose the threshold value in an image. This method is still very effective for thresholding operation and employed by several researchers (Yi et al. (2017),Xu et al. (2016)) to segment nuclei in histopathology images. Otsu had chosen optimal threshold value of an image such that it will maximize inter-class variance or minimize intra-class variance in its histogram. The weighted intra-class variance can be written as equation (4.11).

$$\sigma^2_{intra}(T) = C_1(T)\sigma^2_1(T) + C_2(T)\sigma^2_2(T) \tag{4.11}$$

Where T is the threshold value,$C_1(T)$,$C_2(T)$ are the probabilities of class C_1, C_1 in a bimodal histogram respectively, given in equation (4.12) and (4.13).P_j is the probability

that pixel intensity value has j^{th} intensity level out of L levels.

$$C_1(T) = \sum_{j=1}^{T} P_j \qquad (4.12)$$

$$C_2(T) = \sum_{j=T+1}^{L} P_j \qquad (4.13)$$

Here L is the total no of levels in histogram, in case of gray scale image L=256. j is always integer. $J = 1, 2, 3, \ldots, L$, μ_1,μ_2 are the mean values of class C_1, C_2, in a bimodal histogram respectively, given in equation (4.14) and (4.15).

$$\mu_1 = \sum_{j=1}^{T} (jP_j)/C_1(T) \qquad (4.14)$$

$$\mu_2 = \sum_{j=T+1}^{L} (jP_j)/C_2(T) \qquad (4.15)$$

Corresponding variances $\sigma_1^2(T)$ and $\sigma_2^2(T)$ of class C_1, C_2 in a bimodal histogram are given in equation (4.16) and equation (4.17) respectively.

$$\sigma_1^2(T) = \frac{\sum_{j=1}^{T} (j - \mu_1)^2 P_j}{C_1(T)} \qquad (4.16)$$

$$\sigma_2^2(T) = \frac{\sum_{j=T+1}^{L} (j - \mu_2)^2 P_j}{C_2(T)} \qquad (4.17)$$

Now we have to choose T threshold value optimally such that $\sigma_{intra}^2(T)$, mentioned in equation (4.11), will be minimized. More depth explanation of Otsu thresholding can be found in (Otsu (1979)). In this research, Otsu's threshold is emloyed in order to convert the edge detected image into binary image.

4.2.5   Adaptive Morphology Filter

An adaptive morphological filter has been proposed in order to refine the (binary) segmented image. It can be observed from Figure. 4.3b, that after employing local Otsu's
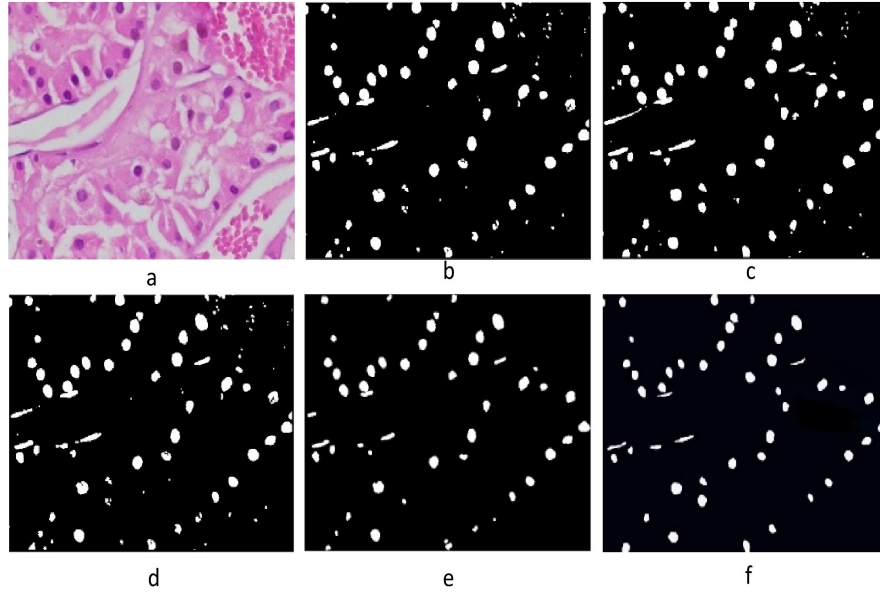
Figure 4.3: a. Source image, b. Binary image after thresholding, c. Final segmented image after conventional morphology filter with disk size a=8, d.Final segmented image after conventional morphology filter with a=2, e. Final segmented image by employed adaptive morphology filter, f. Ground truth

threshold the binary images may have some cluttered small objects. Those small cluttered objects can be the effect of noise. Another possibility is that those are edges of RBC, which are very much similar to nuclei size and shapes in Figure 4.3a. Thus, those small cluttered objects should be removed from the segmented images. Morphological operators (Gonzalez et al. (2004), De Natale and Boato (2017)) like closing or opening operator can remove those kinds of cluttered objects or noise from the segmented binary image.

Opening (De Natale and Boato (2017)) is nothing but an erosion ($B_f \ominus Z$) of a binary image, followed by dilation operation ($B_f \oplus Z$), given in equation (4.18). Where B_f is foreground pixels of binary image I,$z \in a \times a$ is the structuring element. Opening operator can remove small objects (or cluttered nuclei) from segmented binary image.

$$B_f \circ Z = [B_f \ominus Z] \oplus Z \tag{4.18}$$

On the other hand, closing (De Natale and Boato (2017)) is dilation of a binary image, followed by erosion operation. It can fill the small holes or gaps inside a nucleus. The

mathematical expression of closing is given by the following equation (4.19).

$$B_f \bullet Z = [B_f \oplus Z] \ominus Z \qquad (4.19)$$

However, these morphological operators may ruin the shape and boundary structures of nuclei, if the size of structuring element is chosen of higher value. Moreover, we observed that any morphological operator is not robust with the noise present in the binary image. Therefore, we have employed an adaptive morphology filtering operator, in which the size of structuring element is adaptive with the noise present the binary image (after thresholding). The entire in algorithm of morphology filter is given in the Algorithm 3.

Algorithm 3 Algorithm of Adaptive Morphological Filter

```
1. img=imread('Binary image after thresholding')
2. g= 20 or 40
3. gl=np.mean(np.std(img))
4. def imagemorphology(image):
5.    Sz=image.shape
6.    for x in range(Sz[0]-3):
7.        for z in range(Sz[1]-3):
8.            s=g*0.15
9.            sum=0
10.            st2=np.std((image[x:(x+s),z:(z+s)]))
11.            c=c+(st2)/(0.1*Sz[0]*Sz[1])
12.    a= 6-3/ (1+(np.exp (c-gl)/ 0.1))
13.    output= dilation(erosion(image), disk(a)), disk(a))
14.    output2= erosion(dilation(output, disk(a)), disk(a))
15. return output2
16. c=0
17. img2=imagemorphology(img,c)
18. img2=255-(abs(img2))
19. plt.imshow(img3,cmap='Greys')
20. plt.show()
```

---

1. An opening operation, followed by a closing operation is employed for reducing noise and cluttered objects from segmented binary image. Here, the disk length or size of structuring element is not fixed like other conventional morphology operators (Gonzalez et al. (2004)). Rather, it is robust or adaptive with the noise present in the
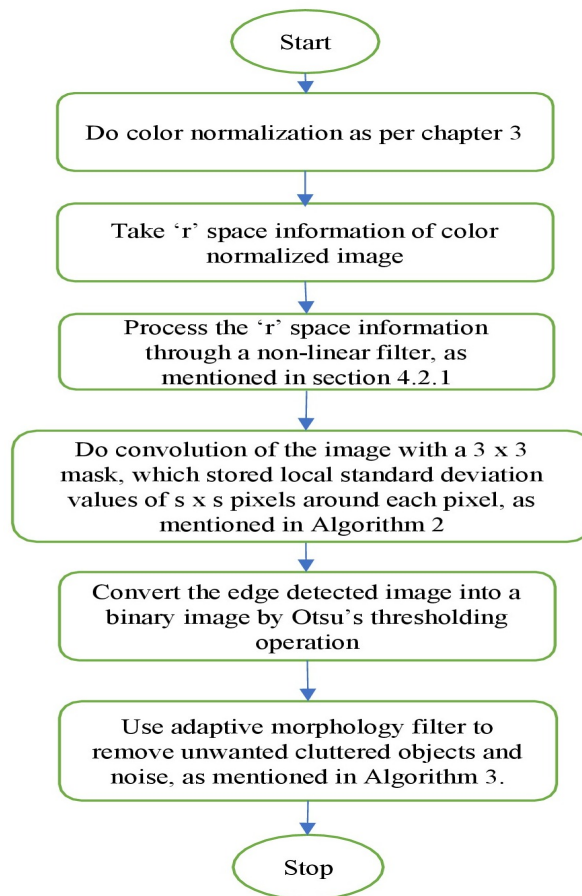
Figure 4.4: Flowchart of entire nuclei segmentation method

histopathology images. This has been observed that the noise inside the histopathology images are correlated with the difference between local standard deviation and global standard deviation. According to our understanding, global standard deviation ($'gl'$ in Algorithm 3) represents overall edge information of the image, since H and E stained histopathology images has unique texture property, which was mentioned in chapter 1. On the other hand, local standard deviation ($'st'$) represents both edge information and noise collectively, to the best of our knowledge. Thus, the difference between these two is somehow correlated with the noise present inside the histopathology image. We have verified this fact universally for all H and E stained histopathology images not only qualitatively but also quantitatively. For that, we took 50 H and E stained histopathology images, thereafter, Gaussian noise are externally added to those images. Moreover, we calculated the difference between global standard deviation and local standard deviation for all images. Thereafter, we observed that inverse of the difference (between local

and global standard deviation) is very much correlated with the PSNR between original image and noisy image. Hence, it is universally verified that noise in H and E stained histopathology images is somehow correlated with the difference between local and global standard deviation.

2. First, function 'c' is calculated which is the sum of all local standard deviation ('st') in a 'sxs' window, given in Algorithm 2. The parameter $(0.1*Sz[0]*Sz[1])$ is the normalization factor, chosen empirically. This normalization factor will push the value of 'c' in the range of global standard deviation 'gl', so that we can subtract those two terms. In our employed morphology filter, a fuzzy function 'a' is incorporated just to control the size of the structuring element. This has been observed that, if the value of 'a' exceed 6, then for some images, nuclei structure was ruined considerably. Similarly, this has also been observed that if $a < 3$, then noise and cluttered objects may be heavily present in final (binary) segmented image. Therefore, maximum and minimum value of 'a' are empirically chosen 6 and 3 respectively. The fuzzy function 'a' which is employed in Algorithm 2, can be generalized by the following equation (4.20).

$$a = a_1 - (a_1 - a_2)/(1 + exp[(c - gl)/(\gamma)]) \qquad (4.20)$$

Here a_1 is the maximum value of a, a_2 is the minimum value of a. Equation (4.20) reveals that employed fuzzy function is a sigmoid function, which is directly proportional to $(c - gl)$, that is, the difference between local and global standard deviation. Therefore, employed fuzzy function is robust with the noise present in histopathology images, to best of our knowledge. Higher the value of $(c - gl)$ indicates that there will be higher chance that the image is affected by noise, thus, at that case, the value of disk length 'a' should be higher and viceversa. Moreover, γ in equation (4.20) is a parameter which controls the fuzziness (smoothness) of the function. If $\gamma = 1$, the fuzzy function will be tending to a straight line. If $0.05 < \gamma < 0.5$, then fuzzy function is observed to be a non-linear function, γ is chosen 0.1 in Algorithm 3, because we wanted to incorporate non-linearity in morphology filter which will reduce more noise from histopathology images. Hence, employed morphology filter is better preserving

72

the shape and structures of nuclei than the conventional fixed morphology operators and at the same time it removes noise and cluttered objects from histopathology images considerably. This can be further observed in Fig.4c, Fig.4d and Fig.4e. The employed morphological filter also works efficiently in a multi-organ dataset, which reveals that the performance of this morphology filter doesn't depend too much on those parameters which are mentioned in Algorithm 3, because the size of the structuring element doesn't change much and it always varies from 3 to 6, due to employing fuzzy function a.

4.2.6   Reasons of choosing unsupervised method

The reason why we didn't employ supervised nuclei segmentation method in this thesis is explained below:

1. In our liver cancer dataset, the number of images is very less (only 80), moreover, in those 80 images we have observed a wide variety of image statistics, especially, in third grade cancer images nuclei size and shape were totally different than that of other images. However, the number of such (third grade cancer) images was only 5 in the entire dataset. Furthermore, in all over the dataset, we have observed the statistical properties of nuclei, other tissues and their patterns are significantly varied per 10 images (approximately). This happened not only because of stain variability, but also, they are not originated from a single cell. Hence, there might be a problem of overfitting if deep neural network was employed for such a dataset. Later, we have compared the performance of proposed method with some of the deep neural methods in the next results and analysis section.

2. Proposed segmentation method is a series of simple image processing techniques which has very low computation complexity than that of any supervised methods, because we don't have to train any dataset.

3. According to our understanding, nuclear segmentation is not basically a supervised problem, because all the nuclei information is already contained in the original image itself. Thus, theoretically no additional ground truth or labelled data should be

Algorithm 4 Algorithm of entire proposed nuclei segmentation method (in open cv2)

```
1. img=imread('Color Normalized Image')
2. r,g,b=cv2.spilt(img)
3. img2=nonlinearfilter(r)
4. g=20 or 40
5. gl=np.mean(np.std(img2))
6. def imagepartition(image,c):
7.     Sz=image.shape
8.     conv(img)=np.zeros(Sz)
9.     for x in range(Sz[0]-12):
10.        for z in range(Sz[1]-12):
11.            s=g*0.15
12.            sum=0
13.            st=np.std((image[x:(x+s),z:(z+s)]))
14.            for i in range(3):
15.               for j in range(3):
16.                   sum=sum + (image [x+i,z+j]*(st))
17.                   if (sum>OtsuThresh):
18.                       sum=1
19.                   else
20.                       sum=0
21.            c= c+st /(0.1*Sz[0]*Sz[1])
22.            conv(img [x,z]) = sum
23.     a= 6-3/ (1+(np.exp (c-gl/ 0.1))
24.     output= dilation(erosion(conv(img)), disk(a)), disk(a))
25.     output2= erosion(dilation(output, disk(a)), disk(a))
26. return output2
27. c=0
28. img3=imagepartition(img2)
29. img3=255-(abs(img3))
30. plt.imshow(img3,cmap='Greys')
31. plt.show()
```

required to perform nuclear segmentation. Indeed, it's just a mapping operation from the original images onto only nuclei portions (blue regions) of those images. Therefore, simple image processing technique is the natural choice for nuclei segmentation of histopathology images.

4.2.7 Combining three Algorithms

In our final proposed nuclei segmentation method we didn't exactly employ only Algorithm 2 and Algorithm 3, mentioned in section 4.2 and 4.32 respectively. Rather we combined all three tasks (that is, edge detection, Otsu thresholding and adaptive morphology filter) into one algorithm in order to reduce computation complexity of the algorithm. That means, those three tasks are not done separately, rather they are implemented inside one 'imagepartition' function, here adptive morphology filter is performed locally, while assigning '0' or '1' to each pixel. The entire algorithm is given in Algorithm 4.

Most of the mathematical notations in Algorithm 4, have already been explored previously in the exaplanations of Algorithm 2 and Algorithm 3.

4.2.8 Results and Analysis

In this section, visual result of the proposed segmentation method is compared with other unsupervised segmentation methods, done by several researchers Xu et al. (2016), Phoulady et al. (2016), Yi et al. (2017) etc. The visual results of edge detected images and final segmented images are shown in Fig.4.2 and Fig.4.5 respectively. Moreover, the performance of proposed segmentation method is compared with two supervised deep learning model, that is, DIST (Naylor et al. (2018)) and MicroNet model (Raza et al. (2019)). The visual results in Fig.5, suggest that the performance of the proposed segmentation method is superior to other unsupervised methods and comparable to deep neural models. All the aforementioned unsupervised methods were implemented by python 3.7, running on an Intel® CoreTMi5 PC with 2.00 GHz CPU and 8 GB RAM.

Whereas, deep neural models were implemented in a NVIDIA Tesla K80 GPU having 12GB (11.439GB Usable) GDDR5 VRAM. For experimentation, 80 number of (40x) liver cancer histopathology images are taken from KMC dataset, which was already mentioned in chater 1. Moreover, in order to validate the effectiveness of proposed algorithm it is also tested on a well known multi-organ dataset (Kumar et al. (2017)), which is readily available in the internet. Furthermore, three quality metrics (F1 score, Jacard index, PSNR) are computed for all segmentation methods with respect to ground truth. The mean value of those quality metrics for liver cancer and multi-organ dataset are presented in Table 4.1 and Table 4.2 respectively.

4.2.9 Quality Metrics for Evaluating Nuclei Segmentation

I. The most frequently used object-based metric F1-score (Kumar et al. (2017)) is employed in order to evaluate the nuclei detection accuracy. The mathematical expression of F1 score is given in equation (4.21).

$$F1 = \frac{2*TP}{2*TP + FP + FN} \qquad (4.21)$$

Here, TP is the number of nuclei truly detected in the segmented image compared with ground truth. FP is the number of nuclei detected falsely, compared with the ground truth. FN is the number of nuclei which are not detected as compared with the ground truth. Here F1 score is calculated as per the algorithm, mentioned in Kumar et al. (2017) which was an assessment with respect to ground truth of the histopathology image. If F1 score is very much closed to 1, this indicates that most of the nuclei in histopathology images are truly detected.

II. A pixel-based quality metric Jaccard index (JI) (Naylor et al. (2018)) is deployed which can measure the similarity of shape or structure of nuclei, between two images, that is ground truth and segmented image. The mathematical expression of Jacard index is given below in equation (4.22). Here, G_j is the jth pixel of nucleus in ground truth

76

image, N_j is the jth pixel of associated nucleus in segmented image.

$$J = \frac{|G_j \cap N_j|}{|G_j \cup N_j|} \tag{4.22}$$

Jaccard index (JI) is very popular metric which is widely employed by other researchers. Closer the value of Jacard index to 1, indicates that the nuclei shape and boundary is exactly matched between ground truth and segmented image.

III. This has been observed that by various segmentation methods, the image is highly affected by noise or artifacts, however, that didn't reflect too much on the metric values of F1 score and Jacard index. Therefore, a metric of Peak Signal to Noise Ratio (PSNR) (Wang and Bovik (2009)) is employed in this research paper in order to find noise level of segmented image, with respect to ground truth image. The mathematical formula for Mean Square Estimation (MSE) and PSNR are given in the following equation (4.23) and (4.24) respectively.

$$MSE(X, Z) = \frac{1}{M} \sum_{j=1}^{M} (X_j - Z_j)^2 \tag{4.23}$$

$$PSNR(X, Z) = 10 log_{10}[L^2/MSE] \tag{4.24}$$

Here, X is the ground truth image, Z is the final segmented image, M is the number of pixels in image, X_j is the jth pixel intensity of ground truth, Z_j is the jth pixel intensity of final segmented image. L is the maximum number of intensity levels in image. Greater the value of PSNR, indicates that the segmented image has lesser noise level with respect to ground truth.

In order to evaluate nuclei segmentation the following must be true:

• F1 score is very much closed to 1, indicates that most of the nuclei in histopathology images are truly detected.

• Closer the value of JI to 1, indicates that nuclei boundary structure and shape is more preserved.

77

• Greater the value of PSNR, indicates that the segmented image has lesser noise level.

Table 4.1: Mean Values of Quality Metrics of 80 **Liver** Cancer Histopathology Images for Various Segmentation Methods

Segmentation Methods	F1Score	JI	PSNR	CPU time (in min)
Xu et al. (2016)	0.7281	0.6877	7.564	1.5
Zhao et al. (2021)	0.8985	0.7747	16.104	25.6
Yi et al. (2017)	0.9312	0.8045	15.445	**1.2**
DIST Naylor et al. (2018)	0.8765	0.7804	14.321	2 days
MicroNet Raza et al. (2019)	0.8632	0.7591	13.499	2 days
Proposed Method (without ColorNorm)	0.9413	0.8233	18.995	4
Proposed Method (with ColorNorm)	**0.9516**	**0.8291**	**19.174**	4.2

Table 4.2: Mean Values of Quality Metrics of 40 **Multiorgan** Histopathology Images for Various Segmentation Methods

Segmentation Methods	F1Score	JI	PSNR	CPU time (in min)
Xu et al. (2016)	0.7518	0.6061	9.661	0.9
Zhao et al. (2021)	0.8314	0.7696	14.014	14.27
Yi et al. (2017)	0.8231	0.7045	13.843	**0.6**
DIST Naylor et al. (2018)	0.7936	0.6621	16.141	2 days
MicroNet Raza et al. (2019)	0.7801	0.6448	14.499	2 days
Proposed Method (without ColorNorm)	0.8573	0.7826	15.757	2.1
Proposed Method (with ColorNorm)	**0.8716**	**0.7923**	**16.321**	2.2

4.2.10   Observation

From Fig.4.2, this can be observed that proposed edge detection method preserved every details of nuclei more efficiently than other existing edge detection methods. Al-Kofahi et al. (2009) and Xu et al. (2016) proposed multi-scale LoG filter in which both of them had chosen the scale of Gaussian filter manually, thus, their method can't work efficiently for every dataset. For implementation of multi-scale edge detection method by Kofahi (Al-Kofahi et al. (2009)), we choose $\sigma_{min} = 4.5$ and $\sigma_{max} = 14.5$ manually, otherwise we didn't get any edge response for liver cancer dataset. For the implementation of gLoG edge detection method, we exactly followed the pseudocode by Xu et al. (2016) which is available in the internet. We only changed the value of α to 0.1, in order to avoid the over-segmentation. Moreover, this can be observed from Fig.2 that, the edge detected image by gLoG is highly affected by noise because they employed a gradient-based edge detection method. Consequently, this can also be observed from Fig.4.5, in the final segmented image by Xu et al. (2016), the nuclei boundary was not exactly preserved as it is they are present in the original image. Table 4.1 also indicates that their method have poor nuclei detection accuracy for liver cancer dataset.

We choose three images from liver cancer dataset in first, second and third column for display purpose, shown in Fig.4.5. These three source images are very special images. Source image in first column has color artifact due to stain variability. Main challenge here is to recover those two nuclei from the stain artifact. Source image in second column is an example of third grade cancer image, thus, there are significant variability of nuclei size and shapes, observed in that image. Therefore, selecting features for nuclei for this source image, is not a very easy task. Moreover, source image in third column is a unique image, because here RBC and some sinusoids' shapes and sizes are very much similar to the same of epithelial nuclei, thus, discriminating nuclei from other tissues will be a difficult task here. Furthermore, two more source images are added from the multi-organ dataset in column 4 and column 5.

From the Fig.4.5, this can be observed that the nuclei segmentation method by Zhao et al. (2021) have done a good job for multi-organ dataset. Consequently, mean value

of F1 score by their method is second best (0.8421) for multi-organ dataset. However, for liver cancer dataset, their method can't detect all the nuclei boundaries clearly, even after employing two refining methods. That happened because of the variability of liver cancer dataset. Consequently, F1 score by their method deviates a bit from 1 for liver dataset, which can be observed from Table 4.1, as well. Overall their method did a decent job for both of the datasets, however, the main limitation of their method is higher computational complexity, which can be further noticed in Table 4.1 and Table. 4.2. The performance of nuclei segmentation method by Yi et al. (2017), is visually good for both liver dataset and multi-organ dataset, except for some of the images (in liver dataset, like in column 3 in Fig.4.5) their algorithm couldn't distinguish between nuclei and other tissues efficiently. Thus, this particular algorithm didn't work efficiently for all images in liver dataset, however, mean value of F1 score by their method is the second best (0.9312) for liver dataset (shown in Table 4.1). This reveals that the overall performance by their method is very decent, despite the fact that they didn't employ any supervised deep neural model.

The results of deep neural models DIST and MicroNet in Fig.4.5 has revealed that both of the methods are working very efficiently for both liver cancer dataset and multi-organ dataset. However, for some of the images, in liver dataset, it couldn't extract nuclei at multi-scale, which can be observed in second column, in Fig.4.5. For training the deep neural models, we employed Xavier initialization for initializing convolutional filter weights. Moreover, we have employed Adam optimizer for calculating the optimal weights during backpropagation. All models are trained for 100 epochs with a batch size of 4. To avoid overfitting we have used early stopping if loss doesn't decrease for 20 epochs. For implementing DIST, in multi-organ dataset, each image was zero padded to make 1024 x 1024 and then were divided into 16 patches of 256 x 256. This generated 384 training, 96 validation and 224 test images including masks. whereas, for MicroNet model, the images were converted to 1008 x 1008, as it uses patches of size 252 x 252. For liver dataset, all full-sized images of size 1440 x 1920 each, have been cropped into 12 patches of 480 x 480 size each. For DIST, we have zero padded the images to make 512 x 512 size each. For Micronet, we have resized the images to 252 x 252 each

and trained on these patches. Furthermore, we performed random data augmentation techniques such as Horizontal flip, vertical flip, random rotation, transpose, random brightness contrast and blurring to deal with overfitting due to limitation of the size of the Kumar dataset and liver dataset. The mean value of quality metrics in Table 4.1 and Table 4.2 suggest that both of the deep neural models worked decently, however, nuclei detection accuracy by their method is still somehow very much deviated from 1. This reveals that indeed employing those deep neural models in such a small dataset (where significant statistical variability appears in both of the datasets) was not so feasible.

On the other hand, in our proposed segmentation method very simple image processing techniques are employed. First a novel edge detection method is proposed, this can be observed from Fig.4.2 that processed image by proposed edge detection method is less affected by noise, since the notion of computing standard deviation is incorporated, instead of computing gradients. Moreover, this can be observed from Fig.4.2 that, proposed edge detection method is capable to extract every little information of nuclei, as they are present in the original image. That means, the shape of nuclei boundary is entirely preserved in most of the images, which may contain significant information of cancer. Moreover, from Fig.4.5 this can be obeserved that final segmented image by proposed method is very closed to groud truth, which is desirable. Furthermore, quality metrics, computed in Table 4.1 and Table 4.2 suggest that performance of proposed segmentation method is superior compared to other segmentation methods. The mean value of F1 score by proposed method is the best (0.9516), compared to other segmentation methods. To the best of our knowledge, proposed segmentation method is the only unsupervised method which achieves nuclei detection accuracy closest to 1. It can also be observed from Table 4.1, that after employing color normalization, F1-score by proposed method has been improved a little bit which justifies the need of color normalization. Indeed, employed color normalization method has utilized contrast enhancement at certain level which has strengthened some of the weak nuclei edges. Moreover, the mean value of Jacard index is the best (0.8291 and 0.7923) by proposed method shown in Table 4.1 and Table 4.2, which suggests that nuclei boundary structure has been significantly preserved by our proposed segmentation method. Furthermore,

PSNR value by our proposed method is also the best (that is, 19.174 and 16.321) shown in Table 4.1 and Table 4.2, which reveals that noise level in the final segmented image by proposed method is the least among all other segmentation methods. Moroever, the main advantage of employing a simple image processing technique in proposed method is that we don't have to do training like other supervised methods, thus, computation complexity is significantly reduced by proposed method compared to other deep neural models (which took approximate 2 days for training).

4.3   Summary

- A novel unsupervised edge detection technique, was proposed for nuclei segmentation of liver cancer H and E stained histopathology images. The notion of computing local standard deviation was incorporated rather than computing gradients.

- Proposed edge detection technique is purely automatic and its performance is not dependent on any parameters, mentioned in the section 4.2.1. To the best of our knowledge, this is the first automatic edge detection method which can extract nuclei edges at multi-scale efficiently from H and E stained histopathology images.

- Unlike other gradient based edge detection, proposed edge detection technique was not very sensitive to noise. A mathematical analysis was also provided in order to prove that noise affected by proposed edge detection method is lesser than that of conventional gradient-based edge detection methods. A quality metric PSNR was also introduced just to measure noise level in the segmented image.

- Edge detected image is further converted into a binary image, by employing Otsu's thresholding operation. Furthermore, an adaptive morphological filter, is employed for refinement of the binary image, in which a non-linear fuzzy function is incorporated. The employment of these three tasks altogether, that is edge detection, Otus's threshold and adaptive morphology are completely new and hadn't been employed before.

- The proposed nuclei segmentation method is also employed to an existing multi-organ dataset, in order to check its effectiveness over wide variety of dataset. The quality metrics had shown that proposed nuclei segmentation method outperformed other existing methods for both of the datasets.
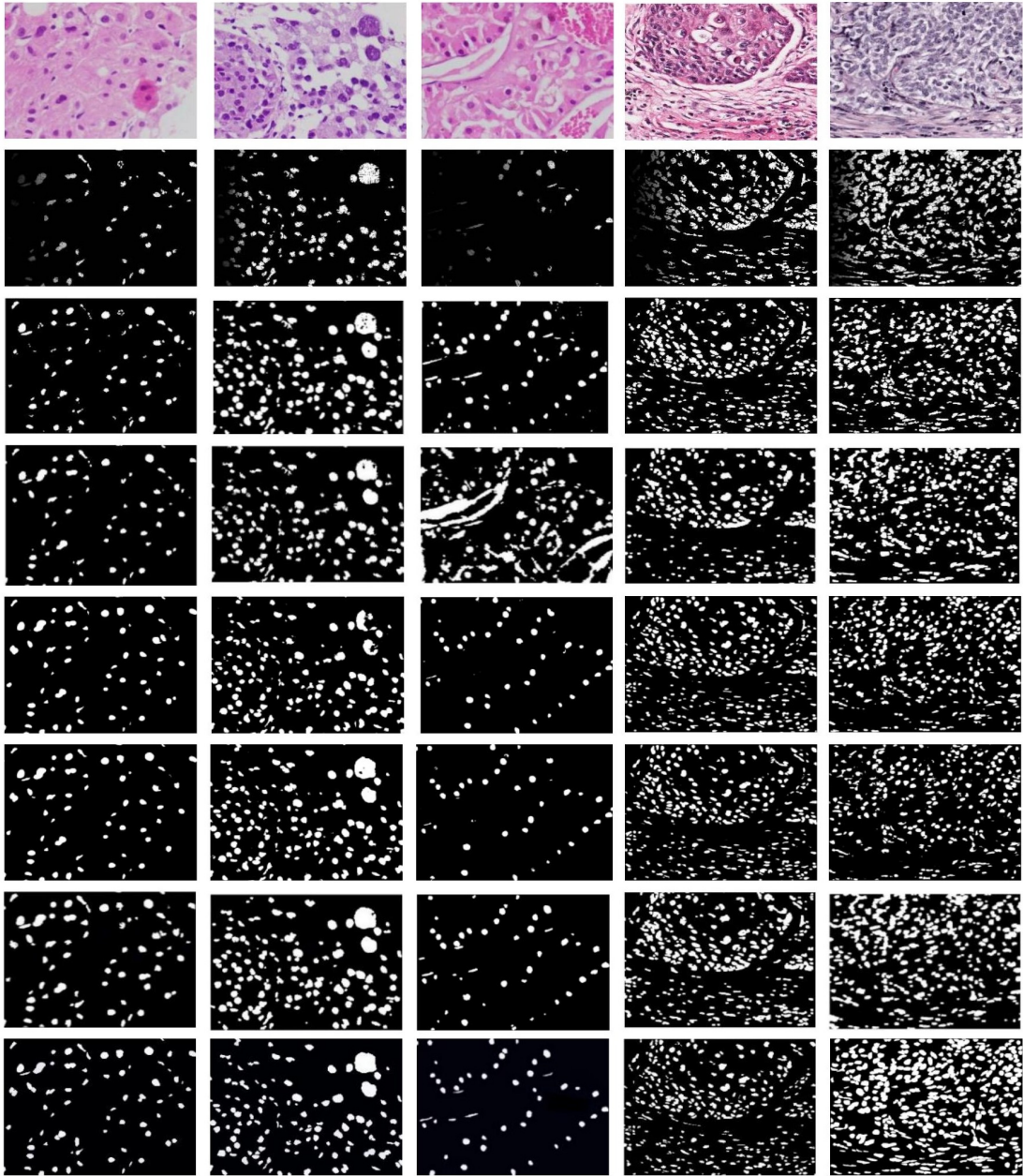
Figure 4.5: Comparison of various nuclei segmentation methods. First three columns represents the liver cancer data, last two columns represent multi-organ data. First row represents the source images. The second row represents the segmented image by Xu et al. (2016) after Watershed transform, third row represents the segmented image by Zhao et al. (2021), fourth row represents the segmented image by Yi et al. (2017), fifth row represents the segmented image by DIST (Naylor et al. (2018)), sixth row represents the segmented image by MicroNet (Raza et al. (2019)), seventh row represents the segmented image by proposed method, 8th row represents the ground truth of segmented image. For proper visualization of images, 2 x zoom is preferable.

CHAPTER 5

Conclusion and Future Work

5.1 Conclusion

In this thesis, first, a global color normalization method was proposed which is modification of Reinhard method. The notion of fuzzy logic was incorporated in order to overcome the limitations of conventional Reinhard method. Our proposed color normalization method is novel, because most of the recent existing color normalization methods are local methods. However, due to unique texture property of H and E stained histopathology images, we proved that global color normalization method is more efficient than local color normalization method. Moreover, due to employing global color transformation, time complexity of our method had been reduced significantly. Furthermore, three quality metrics were introduced in order to evaluate the performance of color normalization, based on the hypotheses. Mathematically, we proved that proposed FMR method had satisfied all three hypotheses as well as we got the best quality metrics compared to other benchmark methods. Hence, we can conclude that our proposed FMR method has outperformed all other existing color normalization methods.

In the second step of CAD, we proposed a novel unsupervised segmentation method for liver cancer H and E stained histopathology images. First, a novel edge detection method, based on computing local standard deviation value, was proposed to extract the edges of nuclei at multi-scale. Proposed edge detection method was more efficiently preserving the nuclei boundary and structure than existing gradient based edge detection method. Moreover, proposed edge detection method was not sensitive to noise, since the notion of standard deviation (of s x s pixels) were deployed rather than computing gradients. Thereafter, the edge detected image is converted into binary image, by Otsu thresholding oerpation, which is followed by a novel adaptive morphology filter in order to refine the segmented image. In novel adaptive morphology filter, size

of the structuring element is robust with the noise present in histopathology images. Resulting image and evaluation of quality metrics suggested that our proposed segmentation method is outperforming the existing unsupervised methods. Moreover, this is also found that the performance of proposed nuclei segmentation method is comparable with the performance of standard deep neural models DIST, MicroNet etc and other recent methods like SEENS.

5.2 Limitations of Proposed Methods

Despite of having the best quality metrics, the performance of our proposed color normalization method is dependent on some parameters, like all the parameters in fuzzy function are chosen empirically. First and third hypotheses will be always true by proposed method and not depending on any parameters. However, the second hypotheses are not always true by proposed method. This can be observed from Table 3.1 and 3.2 that $AMCE_\alpha$ and $AMCE_\beta$ are little bit deviating from zero for some images. Moreover, some of the operations like counting the number of white pixels is more valid for only breast cancer dataset. Because breast have higher number of fatty tissues which creates more white pixels in their H and E stained histopathology images. Therefore, we believe that there is still opportunity to improve the proposed method by incorporating more generalization.

Our edge detection method is entirely a novel method, because it incorporates the notion of standard deviation rather than computing gradients. Our pathologists' group also suggested that the proposed edge detection method is perfectly capable of preserving all the boundary structures and shape of nuclei as it was present in the original image. However, we had to convert the edge detected image into a binary image in order to evaluate the quality metrics, because the ground truth image is itself a binary image. Thus, we had to employ post processing method like OTSU's thresholding operation in order to convert the edge detected image (or grey level image) into a binary image and thereafter refining that binary image by adaptive morphological filter. We

believe that due to incorporating morphology operation there will be always little bit of data loss of nuclei boundaries. However, the edge detected image could be directly fed into the neural network model or into a classifier model in the next step, because all the intensity variation of nuclei has been preserved by the proposed edge detection method. Moreover, by doing that we can reduce the complexity of a deep neural model considerably because the feature space here would be reduced to nuclei portions only.

5.3 Future Work

The future work of this thesis is explained below.

1. Suitable features which are directly correlated to cancerous cells information, should be extracted from the segmented (liver cancer) images. We would prefer to process edge detected (segmented) image, rather than final binary segmented image. Because intensity variation inside a nucleus also contain important information of cancer, according to our pathologists group at KMC, MAHE. Those features can be hand crafted or they can be automatic. In case of Convolutional Neural Network (CNN), the model can automatically learn the complicated features and can update the filter weights accordingly.

2. Thereafter, a supervised classifier (e.g. SVM, CNN like VGG Net, Inception and Resnet model) can be employed in order to classify between cancerous and non-cancerous cells, with higher accuracy. Another kind of classification would be to classify whether the image is associated with 1st grade, 2nd grade or 3rd grade cancer cells. For that, features might be little bit different. For example, if in an image, nuclei size and shape are varying significantly and if the nuclei boundary have irregular texture property, then it's a significant feature of 3rd grade cancer.

3. Proposed Color Normalization method can be employed prior to feeding the images into deep neural network model which may reduce the computation complexity of the classifier a little bit. The proposed color normalization method can also be improved by incorporating some generalization.

REFERENCES

Adams, Rolf and Leanne Bischof (1994), "Seeded region growing." *IEEE Transactions on pattern analysis and machine intelligence*, 16, 641–647.

Aghdasi, Farzin and Rabab K Ward (1996), "Reduction of boundary artifacts in image restoration." *IEEE Transactions on Image Processing*, 5, 611–618.

Al-Kofahi, Yousef, Wiem Lassoued, William Lee, and Badrinath Roysam (2009), "Improved automatic detection and segmentation of cell nuclei in histopathology images." *IEEE Transactions on Biomedical Engineering*, 57, 841–852.

Ali, Sahirzeeshan and Anant Madabhushi (2012), "An integrated region-, boundary-, shape-based active contour for multiple object overlap resolution in histological imagery." *IEEE transactions on medical imaging*, 31, 1448–1460.

Alsubaie, Najah, Nicholas Trahearn, Shan E Ahmed Raza, David Snead, and Nasir M Rajpoot (2017), "Stain deconvolution using statistical analysis of multi-resolution stain colour representation." *PloS one*, 12.

Basu, Mitra (2002), "Gaussian-based edge-detection methods-a survey." *IEEE Transactions on Systems, Man, and Cybernetics, Part C (Applications and Reviews)*, 32, 252–260.

Bejnordi, Babak Ehteshami, Geert Litjens, Nadya Timofeeva, Irene Otte-Höller, André Homeyer, Nico Karssemeijer, and Jeroen AWM van der Laak (2015), "Stain specific standardization of whole-slide histopathological images." *IEEE transactions on medical imaging*, 35, 404–415.

Canny, John (1986), "A computational approach to edge detection." *IEEE Transactions on pattern analysis and machine intelligence*, 679–698.

Celik, Turgay and Tardi Tjahjadi (2011), "Contextual and variational contrast enhancement." *IEEE Transactions on Image Processing*, 20, 3431–3441.

Cheng, Jierong, Jagath C Rajapakse, et al. (2008), "Segmentation of clustered nuclei with shape markers and marking function." *IEEE Transactions on Biomedical Engineering*, 56, 741–748.

Cheuk, Wah, John KC Chan, Tony WH Shek, Julia H Chang, Mei-Hua Tsou, Nancy WF Yuen, Wai-Fu Ng, Alexander CL Chan, and Jaime Prat (2001), "Inflammatory pseudotumor-like follicular dendritic cell tumor: a distinctive low-grade malignant intra-abdominal neoplasm with consistent epstein–barr virus association." *The American journal of surgical pathology*, 25, 721–731.

Dalle, Jean-Romain, Hao Li, Chao-Hui Huang, Wee Kheng Leow, Daniel Racoceanu, and Thomas C Putti (2009), "Nuclear pleomorphism scoring by selective cell nuclei detection." *WACV*.

De Natale, Francesco GB and Giulia Boato (2017), "Detecting morphological filtering of binary images." *IEEE Transactions on Information Forensics and Security*, 12, 1207–1217.

Frigge, Michael, David C Hoaglin, and Boris Iglewicz (1989), "Some implementations of the boxplot." *The American Statistician*, 43, 50–54.

Fukuma, Kiichi, VB Surya Prasath, Hiroharu Kawanaka, Bruce J Aronow, and Haruhiko Takase (2016), "A study on nuclei segmentation, feature extraction and disease stage classification for human brain histopathological images." *Procedia Computer Science*, 96, 1202–1210.

Galon, Jérôme, Anne Costes, Fatima Sanchez-Cabo, Amos Kirilovsky, Bernhard Mlecnik, Christine Lagorce-Pagès, Marie Tosolini, Matthieu Camus, Anne Berger, Philippe Wind, et al. (2006), "Type, density, and location of immune cells within human colorectal tumors predict clinical outcome." *Science*, 313, 1960–1964.

Getreuer, Pascal (2012), "Chan-vese segmentation." *Image Processing On Line*, 2, 214–224.

Ghaznavi, Farzad, Andrew Evans, Anant Madabhushi, and Michael Feldman (2013), "Digital imaging in pathology: whole-slide imaging and beyond." *Annual Review of Pathology: Mechanisms of Disease*, 8, 331–359.

Gonzalez, Rafael C, Richard E Woods, and Steven L Eddins (2004), *Digital image processing using MATLAB*. Pearson Education India.

Graham, Simon, Quoc Dang Vu, Shan E Ahmed Raza, Ayesha Azam, Yee Wah Tsang, Jin Tae Kwak, and Nasir Rajpoot (2019), "Hover-net: Simultaneous segmentation and classification of nuclei in multi-tissue histology images." *Medical Image Analysis*, 58, 101563.

Gurcan, Metin N, Laura E Boucheron, Ali Can, Anant Madabhushi, Nasir M Rajpoot, and Bulent Yener (2009), "Histopathological image analysis: A review." *IEEE reviews in biomedical engineering*, 2, 147–171.

Ham, Jisoo, Yangchi Chen, Melba M Crawford, and Joydeep Ghosh (2005), "Investigation of the random forest framework for classification of hyperspectral data." *IEEE Transactions on Geoscience and Remote Sensing*, 43, 492–501.

Haralick, Robert M (1979), "Statistical and structural approaches to texture." *Proceedings of the IEEE*, 67, 786–804.

Hou, Le, Vu Nguyen, Ariel B Kanevsky, Dimitris Samaras, Tahsin M Kurc, Tianhao Zhao, Rajarsi R Gupta, Yi Gao, Wenjin Chen, David Foran, et al. (2019), "Sparse autoencoder for unsupervised nucleus detection and representation in histopathology images." *Pattern recognition*, 86, 188–200.

Huang, Po-Whei and Yan-Hao Lai (2010), "Effective segmentation and classification for hcc biopsy images." *Pattern Recognition*, 43, 1550–1563.

Irshad, Humayun, Antoine Veillard, Ludovic Roux, and Daniel Racoceanu (2013), "Methods for nuclei detection, segmentation, and classification in digital histopathology: a review—current status and future potential." *IEEE reviews in biomedical engineering*, 7, 97–114.

Ishikawa, Masahiro, Yuri Murakami, Sercan Taha Ahi, Masahiro Yamaguchi, Naoki Kobayashi, Tomoharu Kiyuna, Yoshiko Yamashita, Akira Saito, Tokiya Abe, Akinori Hashiguchi, et al. (2016), "Automatic quantification of morphological features for hepatic trabeculae analysis in stained liver specimens." *Journal of Medical Imaging*, 3, 027502.

Jain, Anil K, Robert P. W. Duin, and Jianchang Mao (2000), "Statistical pattern recognition: A review." *IEEE Transactions on pattern analysis and machine intelligence*, 22, 4–37.

Janowczyk, Andrew, Ajay Basavanhally, and Anant Madabhushi (2017), "Stain normalization using sparse autoencoders (stanosa): application to digital pathology." *Computerized Medical Imaging and Graphics*, 57, 50–61.

Jung, Chanho and Changick Kim (2010), "Segmenting clustered nuclei using h-minima transform-based marker extraction and contour parameterization." *IEEE transactions on biomedical engineering*, 57, 2600–2604.

Jung, Chanho, Changick Kim, Seoung Wan Chae, and Sukjoong Oh (2010), "Unsupervised segmentation of overlapped nuclei using bayesian classification." *IEEE Transactions on Biomedical Engineering*, 57, 2825–2832.

Kass, Michael, Andrew Witkin, and Demetri Terzopoulos (1988), "Snakes: Active contour models." *International journal of computer vision*, 1, 321–331.

Khan, Adnan Mujahid, Nasir Rajpoot, Darren Treanor, and Derek Magee (2014), "A nonlinear mapping approach to stain normalization in digital histopathology images using image-specific color deconvolution." *IEEE Transactions on Biomedical Engineering*, 61, 1729–1738.

Kong, Hui, Hatice Cinar Akakin, and Sanjay E Sarma (2013), "A generalized laplacian of gaussian filter for blob detection and its applications." *IEEE transactions on cybernetics*, 43, 1719–1733.

Kumar, Neeraj, Ruchika Verma, Sanuj Sharma, Surabhi Bhargava, Abhishek Vahadane, and Amit Sethi (2017), "A dataset and a technique for generalized nuclear segmentation for computational pathology." *IEEE transactions on medical imaging*, 36, 1550–1560.

Kumar, Rajesh, Rajeev Srivastava, and Subodh Srivastava (2015), "Detection and classification of cancer from microscopic biopsy images using clinically significant and biologically interpretable features." *Journal of medical engineering*, 2015.

Li, Xingyu and Konstantinos N Plataniotis (2015), "A complete color normalization approach to histopathology images using color cues computed from saturation-weighted statistics." *IEEE Transactions on Biomedical Engineering*, 62, 1862–1873.

Liu, Xinchun, Shidong Chen, Mouyan Zou, and Zhenming Chai (2000), "Edge-detection based on the local variance in angiographic images." *Journal of Electronics (China)*, 17, 338–344.

Macenko, Marc, Marc Niethammer, James S Marron, David Borland, John T Woosley, Xiaojun Guan, Charles Schmitt, and Nancy E Thomas (2009), "A method for normalizing histology slides for quantitative analysis." *2009 IEEE International Symposium on Biomedical Imaging: From Nano to Macro*, 1107–1110, IEEE.

Malladi, Ravi, James A Sethian, and Baba C Vemuri (1995), "Shape modeling with front propagation: A level set approach." *IEEE transactions on pattern analysis and machine intelligence*, 17, 158–175.

Marr, David and Ellen Hildreth (1980), "Theory of edge detection." *Proceedings of the Royal Society of London. Series B. Biological Sciences*, 207, 187–217.

McCann, Michael T (2015), *Tools for automated histology image analysis*. Ph.D. thesis, Carnegie Mellon University.

McCann, Michael T, Joshita Majumdar, Cheng Peng, Carlos A Castro, and Jelena Kovačević (2014a), "Algorithm and benchmark dataset for stain separation in histology images." *2014 IEEE International Conference on Image Processing (ICIP)*, 3953–3957, IEEE.

McCann, Michael T, John A Ozolek, Carlos A Castro, Bahram Parvin, and Jelena Kovacevic (2014b), "Automated histology analysis: Opportunities for signal processing." *IEEE Signal Processing Magazine*, 32, 78–87.

Mosquera-Lopez, Clara, Rodrigo Escobar, and Sos Agaian (2015), "Modeling human-perceived quality for the assessment of digitized histopathology color standardization." *2015 IEEE International Conference on Imaging Systems and Techniques (IST)*, 1–6, IEEE.

Mukherjee, Jayanta and Sanjit K Mitra (2008), "Enhancement of color images by scaling the dct coefficients." *IEEE Transactions on Image processing*, 17, 1783–1794.

Naylor, Peter, Marick Laé, Fabien Reyal, and Thomas Walter (2018), "Segmentation of nuclei in histopathology images by deep regression of the distance map." *IEEE transactions on medical imaging*, 38, 448–459.

Otsu, Nobuyuki (1979), "A threshold selection method from gray-level histograms." *IEEE transactions on systems, man, and cybernetics*, 9, 62–66.

Papoulis, Athanasios and S Unnikrishna Pillai (2002), *Probability, random variables, and stochastic processes*. Tata McGraw-Hill Education.

Parvin, Bahram, Qing Yang, Ju Han, Hang Chang, Bjorn Rydberg, and Mary Helen Barcellos-Hoff (2007), "Iterative voting for inference of structural saliency and characterization of subcellular events." *IEEE Transactions on Image Processing*, 16, 615–623.

Phoulady, Hady Ahmady, Dmitry B Goldgof, Lawrence O Hall, and Peter R Mouton (2016), "Nucleus segmentation in histology images with hierarchical multilevel thresholding." *Medical Imaging 2016: Digital Pathology*, 9791, 979111, International Society for Optics and Photonics.

Plissiti, Marina E and Christophoros Nikou (2012), "Overlapping cell nuclei segmentation using a spatially adaptive active physical model." *IEEE Transactions on Image Processing*, 21, 4568–4580.

Qi, Xin, Fuyong Xing, David J Foran, and Lin Yang (2011), "Robust segmentation of overlapping cells in histopathology specimens using parallel seed detection and repulsive level set." *IEEE Transactions on Biomedical Engineering*, 59, 754–765.

Rabinovich, Andrew, Sameer Agarwal, Casey Laris, Jeffrey H Price, and Serge J Belongie (2004), "Unsupervised color decomposition of histologically stained tissue samples." *Advances in neural information processing systems*, 667–674.

Raza, Shan E Ahmed, Linda Cheung, Muhammad Shaban, Simon Graham, David Epstein, Stella Pelengaris, Michael Khan, and Nasir M Rajpoot (2019), "Micro-net: A unified model for segmentation of various objects in microscopy images." *Medical image analysis*, 52, 160–173.

Reinhard, Erik, Michael Adhikhmin, Bruce Gooch, and Peter Shirley (2001), "Color transfer between images." *IEEE Computer graphics and applications*, 21, 34–41.

Ronneberger, Olaf, Philipp Fischer, and Thomas Brox (2015), "U-net: Convolutional networks for biomedical image segmentation." *International Conference on Medical image computing and computer-assisted intervention*, 234–241, Springer.

Roux, Ludovic, Daniel Racoceanu, Nicolas Loménie, Maria Kulikova, Humayun Irshad, Jacques Klossa, Frédérique Capron, Catherine Genestie, Gilles Le Naour, and Metin N Gurcan (2013), "Mitosis detection in breast cancer histological images an icpr 2012 contest." *Journal of pathology informatics*, 4.

Ruderman, Daniel L, Thomas W Cronin, and Chuan-Chin Chiao (1998), "Statistics of cone responses to natural images: implications for visual coding." *JOSA A*, 15, 2036–2045.

Ruifrok, Arnout C, Dennis A Johnston, et al. (2001), "Quantification of histochemical staining by color deconvolution." *Analytical and quantitative cytology and histology*, 23, 291–299.

Shi, Jianbo and Jitendra Malik (2000), "Normalized cuts and image segmentation." *IEEE Transactions on pattern analysis and machine intelligence*, 22, 888–905.

Song, Youyi, Ling Zhang, Siping Chen, Dong Ni, Baiying Lei, and Tianfu Wang (2015), "Accurate segmentation of cervical cytoplasm and nuclei based on multiscale convolutional network and graph partitioning." *IEEE Transactions on Biomedical Engineering*, 62, 2421–2433.

Tam, Allison, Jocelyn Barker, and Daniel Rubin (2016), "A method for normalizing pathology images to improve feature extraction for quantitative pathology." *Medical physics*, 43, 528–537.

Vahadane, Abhishek, Tingying Peng, Amit Sethi, Shadi Albarqouni, Lichao Wang, Maximilian Baust, Katja Steiger, Anna Melissa Schlitter, Irene Esposito, and Nassir Navab (2016), "Structure-preserving color normalization and sparse stain separation for histological images." *IEEE transactions on medical imaging*, 35, 1962–1971.

Vincent, Luc and Pierre Soille (1991), "Watersheds in digital spaces: an efficient algorithm based on immersion simulations." *IEEE Transactions on Pattern Analysis & Machine Intelligence*, 583–598.

Wang, Zhou and Alan C Bovik (2002), "A universal image quality index." *IEEE signal processing letters*, 9, 81–84.

Wang, Zhou and Alan C Bovik (2009), "Mean squared error: Love it or leave it? a new look at signal fidelity measures." *IEEE signal processing magazine*, 26, 98–117.

Wang, Zhou, Alan C Bovik, Hamid R Sheikh, and Eero P Simoncelli (2004), "Image quality assessment: from error visibility to structural similarity." *IEEE transactions on image processing*, 13, 600–612.

Xing, Fuyong and Lin Yang (2016), "Robust nucleus/cell detection and segmentation in digital pathology and microscopy images: a comprehensive review." *IEEE reviews in biomedical engineering*, 9, 234–263.

Xu, Hongming, Cheng Lu, Richard Berendt, Naresh Jha, and Mrinal Mandal (2016), "Automatic nuclei detection based on generalized laplacian of gaussian filters." *IEEE journal of biomedical and health informatics*, 21, 826–837.

Xu, Hongming, Cheng Lu, and Mrinal Mandal (2014), "An efficient technique for nuclei segmentation based on ellipse descriptor analysis and improved seed detection algorithm." *IEEE journal of biomedical and health informatics*, 18, 1729–1741.

Yi, Faliu, Junzhou Huang, Lin Yang, Yang Xie, and Guanghua Xiao (2017), "Automatic extraction of cell nuclei from h&e-stained histopathological images." *Journal of Medical Imaging*, 4, 027502.

Zhao, Meng, Hao Wang, Ying Han, Xiaokang Wang, Hong-Ning Dai, Xuguo Sun, Jin Zhang, and Marius Pedersen (2021), "Seens: Nuclei segmentation in pap smear images with selective edge enhancement." *Future Generation Computer Systems*, 114, 185–194.

LIST OF PAPERS BASED ON THESIS

1. **Santanu Roy**, Alok.K.Jain, Shyam Lal, J. Kini, "A study about color normalization methods for histopathology images", *Micron (Elsevier)*, vol. 114, pp. 42-62, November 2018, Indexed by SCI, Impact Factor: 1.782, **(published)**

2. **Santanu Roy**, Shyam Lal, J. Kini "A Novel Color Normalization Method for Hematoxylin and Eosin Histopathology Images", *IEEE Access Journal*, vol. 7, pp. 28982-28998, Feb 2019, Indexed by SCI, Impact Factor: 4.089 **(published)**

3. **Santanu Roy**, Devikalyan Das, Shyam Lal, J. Kini, "A Novel Edge Detection Method for Nuclei Segmentation of Liver Cancer Histopathology Images", *Journal of Ambient Intelligence and Humanized Computing*, Indexed by SCI, Impact Factor: 4.594, **(paper is accepted)**

CURRICULUM VITAE

Name	Santanu Roy
Address	22/1, Tentul Beria Garia Station Road
	P.O. Garia, Kolkata- 700084
	West Bengal, India
E-mail	santanuroy35@gmail.com
Qualification	• M.Tech | Information and Communication Technology (ICT) | DA-IICT, Gandhinagar, Gujarat
	• B.Tech | Electronics and Communication Engineering (ECE) | WBUT, Kolkata